

AD-A256 831

2



# NAVAL POSTGRADUATE SCHOOL Monterey, California



SDTIC  
ELECTE  
NOV 06 1992  
S E D

## THESIS

PREDICTION OF TURBINE CASCADE FLOWS WITH A  
QUASI-THREE-DIMENSIONAL ROTOR VISCOUS CODE AND  
THE EXTENSION OF THE ALGEBRAIC TURBULENCE  
MODEL

by

Wang, Chun-Wei

Thesis Advisor:

Garth V. Hobson

Approved for public release; distribution is unlimited

92-29050



251450

69097

| REPORT DOCUMENTATION PAGE  |  |   |                             |
|--|--|---|-----------------------------|
| 1a. REPORT SECURITY CLASSIFICATION<br>UNCLASSIFIED   |  | 1b. RESTRICTIVE MARKINGS  |                             |
| 2a. SECURITY CLASSIFICATION AUTHORITY  |  | 3. DISTRIBUTION/AVAILABILITY OF REPORT<br>Approved for public release; distribution is unlimited. |                             |
| 2b. DECLASSIFICATION/DOWNGRADING SCHEDULE  |  |   |                             |
| 4. PERFORMING ORGANIZATION REPORT NUMBER(S)  |  | 5. MONITORING ORGANIZATION REPORT NUMBER(S)   |                             |
| 6a. NAME OF PERFORMING ORGANIZATION<br>Naval Postgraduate School   | 6b. OFFICE SYMBOL<br>(If applicable)<br>33 | 7a. NAME OF MONITORING ORGANIZATION<br>Naval Postgraduate School                                  |                             |
| 6c. ADDRESS (City, State, and ZIP Code)<br>Monterey, CA 93943-5000   |  | 7b. ADDRESS (City, State, and ZIP Code)<br>Monterey, CA 93943-5000                                |                             |
| 8a. NAME OF FUNDING/SPONSORING ORGANIZATION  | 8b. OFFICE SYMBOL<br>(If applicable)       | 9. PROCUREMENT INSTRUMENT IDENTIFICATION NUMBER   |                             |
| 8c. ADDRESS (City, State, and ZIP Code)  |  | 10. SOURCE OF FUNDING NUMBERS   |                             |
|  |  | Program Element No.   | Project No.                 |
|  |  | Task No.  | Work Unit Accession Number  |
| 11. TITLE (Include Security Classification)<br>PREDICTION OF TURBINE CASCADE FLOWS WITH A QUASI-THREE-DIMENSIONAL ROTOR VISCOUS CODE AND THE EXTENSION OF THE ALGEBRAIC TURBULENCE MODEL   |  |   |                             |
| 12. PERSONAL AUTHOR(S) Wang, Chun-Wei  |  |   |                             |
| 13a. TYPE OF REPORT<br>Master's Thesis   | 13b. TIME COVERED<br>From To               | 14. DATE OF REPORT (year, month, day)<br>June 1992  | 15. PAGE COUNT<br>72        |
| 16. SUPPLEMENTARY NOTATION<br>The views expressed in this thesis are those of the author and do not reflect the official policy or position of the Department of Defense or the U.S. Government.   |  |   |                             |
| 17. COSATI CODES   |  | 18. SUBJECT TERMS (continue on reverse if necessary and identify by block number)                 |                             |
| FIELD  | GROUP                                      | SUBGROUP  |                             |
|  |  | RVCQ3D, Turbulence Models   |                             |
| 19. ABSTRACT (continue on reverse if necessary and identify by block number)   |  |   |                             |
| <p>A quasi-three-dimensional rotor viscous code is used to predict high subsonic flow through an annular cascade of turbine blades. The well known Baldwin-Lomax turbulence model is used in the program. An attempt was made to implement a new turbulence model, based on renormalization group theory in the program. This was done to improve the prediction of the boundary layer transition on the blade surfaces and subsequent wake development. The comparison of these two turbulence models with experimental data are presented. Pressure, velocity ratio, flow angle distributions and downstream wake predictions were studied using results from RVCQ3D (Rotor Viscous Code Quasi-Three-Dimensional) code. The computed results showed good agreement with experiment when comparing the blade surface local static pressure to inlet total pressure ratio at the midspan position of the annular turbine cascade. The computational approach used to implement the turbulence model is also described.</p> |  |   |                             |
| 20. DISTRIBUTION/AVAILABILITY OF ABSTRACT<br><input checked="" type="checkbox"/> UNCLASSIFIED/UNLIMITED <input type="checkbox"/> SAME AS REPORT <input type="checkbox"/> DTIC USERS  |  | 21. ABSTRACT SECURITY CLASSIFICATION<br>UNCLASSIFIED  |                             |
| 22a. NAME OF RESPONSIBLE INDIVIDUAL<br>Garth V. Hobson   |  | 22b. TELEPHONE (Include Area code)<br>(408)646-2888   | 22c. OFFICE SYMBOL<br>AA/HG |

Approved for public release; distribution is unlimited.

**PREDICTION OF TURBINE CASCADE FLOWS WITH A  
QUASI-THREE-DIMENSIONAL ROTOR VISCOUS CODE AND  
THE EXTENSION OF THE ALGEBRAIC TURBULENCE MODEL**

by

**Wang, Chun-Wei  
Lieutenant, Republic of China Navy  
B.S., Chung-Cheng Institute of Technology**

**Submitted in partial fulfillment  
of the requirements for the degree of**

**MASTER OF SCIENCE IN AERONAUTICAL ENGINEERING**

from the

**NAVAL POSTGRADUATE SCHOOL  
June, 1992**

**Author:**

\_\_\_\_\_  
**Wang, Chun-Wei**

**Approved by:**

*Garth V. Hobson*  
\_\_\_\_\_  
**Garth V. Hobson, Thesis Advisor**

*Raymond P. Shreeve*  
\_\_\_\_\_  
**Raymond P. Shreeve, Second Reader**

*Daniel J. Collins*  
\_\_\_\_\_  
**Daniel J. Collins, Chairman**  
**Department of Aeronautics and Astronautics**

**ABSTRACT**

A quasi-three-dimensional rotor viscous code is used to predict high subsonic flow through an annular cascade of turbine blades. The well known Baldwin-Lomax turbulence model is used in the program. An attempt was made to implement a new turbulence model, based on renormalization group theory in the program. This was done to improve the prediction of the boundary layer transition on the blade surfaces and subsequent wake development. The comparison of these two turbulence models with experimental data are presented. Pressure, velocity ratio, flow angle distributions and downstream wake predictions were studied using results from RVCQ3D (Rotor Viscous Code Quasi-Three-Dimensional) code. The computed results showed good agreement with experiment when comparing the blade surface local static pressure to inlet total pressure ratio at the midspan position of the annular turbine cascade. The computational approach used to implement the turbulence model is also described.

**DTIC QUALITY INSPECTED 4**

|                     |                                     |
|---------------------|-------------------------------------|
| Accession For       |                                     |
| NTIS CRA&I          | <input checked="" type="checkbox"/> |
| DTIC TAB            | <input type="checkbox"/>            |
| Unannounced         | <input type="checkbox"/>            |
| Justification ..... |                                     |
| By .....            |                                     |
| Distribution /      |                                     |
| Availability Codes  |                                     |
| Dist                | Avail and/or Special                |
| A-1                 |                                     |

## TABLE OF CONTENTS

|      |   |    |
|------|---|----|
| I.   | INTRODUCTION . . . . .                                | 1  |
|      | A. BACKGROUND . . . . .                               | 1  |
|      | B. PURPOSE . . . . .                                  | 3  |
| II.  | FORMULATION . . . . .                                 | 6  |
|      | A. GOVERNING EQUATIONS . . . . .                      | 6  |
|      | B. TURBULENCE MODEL . . . . .                         | 8  |
|      | 1. BALDWIN-LOMAX MODEL . . . . .                      | 8  |
|      | 2. RNG MODEL . . . . .                                | 11 |
| III. | SOLUTION METHOD . . . . .                             | 16 |
|      | A. GRID GENERATION . . . . .                          | 16 |
|      | B. NUMERICAL SCHEME . . . . .                         | 17 |
|      | C. BOUNDARY CONDITIONS . . . . .                      | 18 |
| IV.  | RESULTS AND DISCUSSION . . . . .                      | 20 |
|      | A. STREAMTUBE VARIATION AND GRID RESOLUTION . . . . . | 22 |
|      | 1. STREAMTUBE VARIATION . . . . .                     | 22 |
|      | 2. GRID RESOLUTION . . . . .                          | 25 |

|                            |   |    |
|----------------------------|---|----|
| B.                         | B-L MODEL AND RNG MODEL . . . . .             | 29 |
| 1.                         | BLADE SURFACE PRESSURE DISTRIBUTION . . . . . | 33 |
| 2.                         | MIDCHORD FLOWFIELD COMPARISON . . . . .       | 35 |
| 3.                         | WAKE PREDICTION . . . . .                     | 38 |
| C.                         | DISCUSSION . . . . .                          | 39 |
| V.                         | CONCLUSION . . . . .                          | 44 |
| APPENDIX A                 | DATA FOR GOLDMAN'S CASCADE . . . . .          | 46 |
| APPENDIX B                 | RESULTS USING A 97 X 31 GRID . . . . .        | 49 |
| APPENDIX C                 | T106 [Ref. 19] TEST CASE . . . . .            | 53 |
| LIST OF REFERENCES         | . . . . .                                     | 57 |
| INITIAL DISTRIBUTION LIST. | . . . . .                                     | 59 |

## NOMENCLATURE

- A<sup>+</sup> - Damping coefficient
- c - Speed of sound
- C<sub>d</sub> - Drag coefficient
- C<sub>p</sub> - Specific heat at constant pressure
- C<sub>v</sub> - Specific heat at constant volume
- E - Energy spectrum
- e - Total energy per unit volume
- H - Enthalpy
- J - Jacobian
- k - Wavenumber
- L - Chord length
- l - Mixing length
- L<sub>r</sub> - Length scale
- m - Meridional direction
- n - Normal distance from boundary
- p - Static pressure
- Pr - Prandtl number
- Q - Total velocity
- R - Gas constant
- Re - Reynolds number
- S - Mean strain rate squared
- s - Distance from the trailing edge
- T - Temperature

- t - Time
- u - x direction velocity component
- v - y direction velocity component
- $y^+$  - Normalized surface distance
- $\gamma$  - Specific heat ratio
- $\delta$  - Boundary layer thickness
- $\varepsilon$  - Dissipation rate of turbulence
- $\kappa$  - Von Karman's constant
- $\Lambda_T$  - Infrared cutoff wavenumber
- $\lambda$  - Thermal conductivity
- $\mu$  - Dynamic viscosity
- $\nu$  - Renormalized or effective eddy viscosity
- $\nu_0$  - Molecular kinematic viscosity
- $\rho$  - Density
- $\tau$  - Shear stress
- $\omega$  - Vorticity

Subscripts

- m - Meridional
- t - Turbulent
- x - Axial
- W - At the wall
- $\theta$  - Tangential (circumferential) direction

Superscripts

- \* - Normalization constant
- ' - Divided by density

|           |   |    |
|-----------|---|----|
| Figure 19 | Shear strain rate and vorticity distribution normal to the suction surface . . . . .                        | 43 |
| Figure A1 | Geometry of C-type 250 X 60 grid . . . . .  | 47 |
| Figure A2 | The streamtube variation data . . . . .   | 48 |
| Figure B1 | Effect of streamtube variation on convergence history for the 97 X 31 grid . . . . .                        | 50 |
| Figure B2 | Effect of streamtube variation on static pressure to inlet total pressure ratio . . . . .                   | 51 |
| Figure B3 | Effect of streamtube variation on wake velocity to critical velocity ratio . . . . .                        | 52 |
| Figure C1 | Geometry of the subsonic turbine cascade, T106 . . . . .  | 54 |
| Figure C2 | Initial prediction of the blade surface static pressure coefficient distribution around the blade . . . . . | 55 |
| Figure C3 | Initial prediction of the skin friction coefficient distribution on the blade surface . . . . .             | 56 |

## I. INTRODUCTION

### A. BACKGROUND

The term renormalization belongs to quantum physics. It arises when the discrete formulation for particles is extended to include the case of continuous fields. Initially this is done by formulating the discrete problem on a lattice. In turbulence theory, when the continuum limit is taken, and the Kolmogorov spectrum hypotheses are applied in the wavenumber space, the infrared divergence of turbulence theory arises. Renormalization is a standard method of removing the resulting singularities and this procedure is described in McComb [Ref. 1].

In an earlier paper [Ref. 2], Yakhot and Orszag have proposed the application of renormalization group theory to turbulence modelling. In the RNG approach, the Reynolds stresses are accounted for by repeatedly recasting the equation of motion with the smallest spatial scales represented by effective larger scale motions. Following each renormalization, the spectrum is narrowed by removal of a band of the highest remaining frequencies. When the process is complete, a set of averaged equations are obtained along with equations for an effective turbulent viscosity.

Lund [Ref. 3] used an algebraic mixing-length model to calculate provisional values of eddy viscosity at each point normal to the wall. These provisional values are then processed by the RNG equation and the actual values of eddy viscosity to be used in the mean-flow calculation are determined. The RNG equation is such that if the provisional value of the eddy viscosity is below a certain threshold value, which is determined by the Heaviside function, the eddy viscosity will be zero. As the provisional values of eddy viscosity increase above the threshold, the RNG equation returns non-zero values of eddy viscosity that are always less than the provisional values. Since the provisional values of eddy viscosity increase with Reynolds number, the RNG eddy viscosity will be zero for low Reynolds numbers, increase for moderate Reynolds numbers, and finally asymptote to a fully turbulent value for large Reynolds numbers. This type of behavior should make the RNG approach well suited for transition calculations. The heart of the algebraic RNG model is a ramp function that switches on when the provisional value of eddy viscosity is above the threshold. If the ramp function is on, the RNG equation takes the form of a cubic equation to be solved for the eddy viscosity. Lund also mentioned a transformation of the cubic equation to a quartic equation and that this form of the RNG model would possibly be more robust.

Kirtley [Ref. 4] used a similar quartic equation to study complex three-dimensional turbomachinery flows. As

the RNG equation was expressed as a function of mean strain rate, the model was then referred to as "energy-based". In the procedure of solving the eddy viscosity, the shear stress was introduced into the quartic equation and a modified mixing length was applied in the wake region. Newton's method was used to find the roots of the RNG equation, with the shear stress determined from a previous value of eddy viscosity.

## **B. PURPOSE**

The aim of this thesis is to improve the viscous flow analysis in turbomachinery blade rows. The Navier-Stokes equations need to be solved and these are simplified by Reynolds averaging which gives rise to the Reynolds stress tensor in the momentum equations. Turbulence models are needed to account for the Reynolds stress tensor, and these represent the transport of momentum due to turbulent fluctuations. Good turbulence models have been developed for relatively narrow ranges of flows with excellent accuracy, but they can not be applied with confidence to complex flows.

For computational efficiency and code simplicity, the Baldwin-Lomax algebraic turbulence model works very well for many two-dimensional flows. This model calculates the viscosity induced by the vorticity. However, it contains many empirically determined constants, which are determined from simple two-dimensional shear-flow experiments. These constants

are the near-wall damping of turbulence, transition location, and intermittency. In the analysis of turbine flow fields, the transition region of the boundary layer occupies most of the suction-side surface. The predictions of skin friction and heat transfer are important in turbine blades, therefore, less reliance on empiricism is desired.

The RNG formalism, cannot as yet account for free-stream-turbulence intensity effects. The elimination of infinitesimally thin high-wavenumber bands is repeated over the renormalized spectrum, giving rise to recurrence relations which link the low-Reynolds-number regions of the turbulence with the high. Some constants appear in these relations but they are determined analytically from assumptions about the shape of the energy spectrum. The eddy viscosity is a function of the mean strain rate.

The object of this study is to apply the RNG turbulence model into the Rotor Viscous Code Quasi-3-D (RVCQ3D) [Ref.5 and Ref.6] and the comparison of the results to those computed with the Baldwin-Lomax turbulence model. Quasi-three-dimensional flow is computed by numerically solving the thin-layer Navier-Stokes equations using a multi-stage Runge-Kutta scheme with a spatially varying time step and implicit residual smoothing.

This study entailed the computation of two cascade test cases. The first test case is an annular cascade of turbine stator blades which was experimentally measured by Goldman and

Seasholtz [Ref.7] with a one-component laser Doppler velocimeter. They mapped out the flow at various radial and axial stations by performing pitchwise blade-to-blade and wake surveys. RVCQ3D was used to compute the midspan location and comparisons were made with the experimental measurements.

The second test case is a subsonic cascade of turbine rotor blades, experimentally investigated by Hoheisel [Ref.8]. The wake traverse measurements were performed with a wedge type probe, and the boundary layer measurements were carried out on the blade suction surface with a flattened Pitot probe. This test case was only computed with the Baldwin-Lomax turbulence model and is presented as an Appendix.

## II. FORMULATION

### A. GOVERNING EQUATIONS

The mass-averaged, compressible form of the Navier-Stokes equations theoretically model turbulent flow. The equations are solved numerically on a body-conforming grid system, so these equations are transformed from the Cartesian system  $(x, y)$  to a body-fitted coordinate system  $(\xi, \eta)$ . The thin-layer approximation which neglects the viscous-diffusion terms parallel to the body surface is applied after the transformation.

Liu, Sockol, and Prah [Ref.9] defined the nondimensionalized reference quantities as follows:

$$\begin{aligned}\bar{t} &= \frac{t}{\left(\frac{L}{c^*}\right)}, & \bar{x} &= \frac{x}{L}, & \bar{y} &= \frac{y}{L}, \\ \bar{u} &= \frac{u}{c^*}, & \bar{v} &= \frac{v}{c^*}, & \bar{p} &= \frac{p}{(\rho_0 c^{*2})}, \\ \bar{T} &= \frac{T}{T_0}, & \bar{e} &= \frac{e}{(\rho_0 c^{*2})}, & & (1) \\ \bar{\rho} &= \frac{\rho}{\rho_0}, & \bar{\mu} &= \frac{\mu}{\mu_0}, \\ c^* &= \sqrt{\frac{2\gamma RT_0}{\gamma+1}}, & Re &= \frac{\rho_0 c^* L}{\mu_0}, & Pr &= \frac{\mu_0 C_p}{\lambda}\end{aligned}$$

The nondimensionalized, conservative form of the two-dimensional, time-dependent, mass-averaged, thin-layer Navier-Stokes equations, from Chima [Ref. 5], are as follows (omitting the overbar):

$$\frac{\partial}{\partial t} (J^{-1}F_0) + J \frac{\partial}{\partial \xi} (J^{-1}F_1) + J \frac{\partial}{\partial \eta} (J^{-1}F_2) - \frac{1}{Re} J \frac{\partial}{\partial \eta} (J^{-1}F_4) = F_3 \quad (2)$$

where  $J$  is the transformation Jacobian given by

$$J = \begin{vmatrix} \frac{\partial x}{\partial \xi} & \frac{\partial x}{\partial \eta} \\ \frac{\partial y}{\partial \xi} & \frac{\partial y}{\partial \eta} \end{vmatrix} \quad (3)$$

Equation (2) can be rewritten as follows:

$$\frac{\partial}{\partial t} (\hat{F}_0) + \frac{\partial}{\partial \xi} (\hat{F}_1) + \frac{\partial}{\partial \eta} (\hat{F}_2) - \frac{1}{Re} \frac{\partial}{\partial \eta} (\hat{F}_4) = \hat{F}_3 \quad (4)$$

to which the numerical scheme is applied.

$$F_0 = \begin{pmatrix} \rho \\ \rho u \\ \rho v \\ e \end{pmatrix} \quad F_1 = \begin{pmatrix} \rho u U + \xi_x p \\ \rho v U + \xi_y p \\ (e+p) U \end{pmatrix} \quad F_2 = \begin{pmatrix} \rho v V + \eta_x p \\ \rho u V + \eta_y p \\ (e+p) V \end{pmatrix} \quad F_3 = \begin{pmatrix} 0 \\ 0 \\ 0 \\ 0 \end{pmatrix} \quad (5)$$

$$F_4 = \begin{pmatrix} 0 \\ m_1 u_\eta + m_2 v_\eta \\ m_2 u_\eta + m_3 v_\eta \\ m_4 \left[ \frac{e}{p} - \frac{1}{2} (u^2 + v^2) \right]_\eta + (m_1 u + m_2 v) u_\eta + (m_2 u + m_3 v) v_\eta \end{pmatrix}$$

where

$$\begin{aligned}m_1 &= \left(\frac{4}{3}\eta_x^2 + \eta_y^2\right) (\mu + \mu_t) \\m_2 &= \frac{1}{3}\eta_x\eta_y (\mu + \mu_t) \\m_3 &= \left(\eta_x^2 + \frac{4}{3}\eta_y^2\right) (\mu + \mu_t) \\m_4 &= (\eta_x^2 + \eta_y^2) \left(\frac{\mu}{Pr} + \frac{\mu_t}{Pr_t}\right)\end{aligned}\tag{6}$$

and

$$e = \rho \left[ C_v T + \frac{1}{2}(u^2 + v^2) \right]\tag{7}$$

$$p = (\gamma - 1) \left[ e - \frac{1}{2}\rho(u^2 + v^2) \right]\tag{8}$$

$$\begin{aligned}U &= u \xi_x + v \xi_y \\V &= u \eta_x + v \eta_y\end{aligned}\tag{9}$$

## B. TURBULENCE MODEL

### 1. BALDWIN-LOMAX MODEL

This model is a two-layer algebraic eddy viscosity model proposed by Baldwin and Lomax [Ref.10], and has been extensively used for calculating turbulent flows. The description of the model follows.

The eddy viscosity is calculated using

$$\mu_t = \begin{cases} (\mu_t)_{inner} & \text{if } y \leq y_{crossover} \\ (\mu_t)_{outer} & \text{if } y > y_{crossover} \end{cases} \quad (10)$$

where  $y_{crossover}$  is given by the minimum value of  $y$  for which  $(\mu_t)_{inner} = (\mu_t)_{outer}$ .

The inner and outer values are given by

$$(\mu_t)_{inner} = \rho (\kappa y (1 - e^{-\frac{y^*}{A^*}}))^2 |\omega| \quad (11)$$

$$(\mu_t)_{outer} = C_{outer} \rho F_{WAKE} F_{KLEB} \quad (12)$$

where

$$y^* = \frac{\sqrt{\rho_N \tau_N y}}{\mu_N} \quad (13)$$

$A^* = 26$ ,  $C_{outer} = 0.0269$ , and  $F_{WAKE}$  is given by

$$F_{WAKE} = \min(y_{max} F_{max}, 0.25 y_{max} V_{DIF}^2 / F_{max}) \quad (14)$$

The quantities  $y_{max}$  and  $F_{max}$  are found from

$$F(y) = y |\omega| (1 - e^{-\frac{y^*}{A^*}}) \quad (15)$$

where  $y_{max}$  is the  $y$  value for which  $F(y)$  is a maximum.

$F_{KLEB}$  is given by

$$F_{KLEB} = [1 + 5.5 \left( \frac{0.3 Y}{y_{max}} \right)^6]^{-1} \quad (16)$$

The term  $v_{DIP}$  is given by

$$v_{DIP} = (\sqrt{v_0^2 + v_m^2})_{max} - (\sqrt{v_0^2 + v_m^2})_{min} \quad (17)$$

Except for wakes, the second term is zero.

A mixing length is introduced in the inner viscosity equation, as follows;

$$l = \kappa y (1 - e^{-\frac{y}{\lambda^*}}) \quad (18)$$

and the  $\omega$  term is obtained from the vorticity, as:

$$\omega = \frac{1}{2} (\text{vorticity}) = \frac{1}{2} \left( \frac{\partial v}{\partial x} - \frac{\partial u}{\partial y} \right) \quad (19)$$

Since the coordinates are transformed from  $(x, y)$  to  $(\xi, \eta)$ , the vorticity in the equation above becomes

$$\frac{\partial v}{\partial x} - \frac{\partial u}{\partial y} = \frac{1}{J} \left[ (y_\eta \frac{\partial v}{\partial \xi} - y_\xi \frac{\partial v}{\partial \eta}) - (-x_\eta \frac{\partial u}{\partial \xi} + x_\xi \frac{\partial u}{\partial \eta}) \right] \quad (20)$$

From this vorticity form, the eddy viscosity can be calculated by combining the inner and outer turbulent viscosities.

## 2. RNG MODEL

In Kirtley [Ref. 4], the following relation for the renormalized viscosity is derived:

$$\begin{aligned} \nu &= \nu_0 [1 + H(\frac{a}{\nu_0^3} \epsilon \Lambda_f^{-4} - C_c)]^{\frac{1}{3}} \\ &= \nu_0 [1 + H(\frac{\epsilon}{\nu_0^3} L_f^4 - C_c)]^{\frac{1}{3}} \end{aligned} \quad (21)$$

where  $H(x)$  is the Heaviside function, which is zero for negative  $x$  and equal to  $x$  for all positive  $x$ .  $\Lambda_f$  is the wavenumber corresponding to the largest length scale in the inertial range. The coefficient  $a = 0.1186$  and was derived [Ref. 2] from the  $-5/3$  power law for the turbulence energy spectrum.  $C_c$  is a function of both  $a$  and the ultraviolet dissipation range cut-off in the spectrum of turbulence; the suggested range is between 75 and 200. The dissipation rate of turbulence is determined from the following equations:

$$\epsilon = \nu S \quad (22)$$

where

$$\begin{aligned} S &= \left( \frac{\partial u_i}{\partial x_j} + \frac{\partial u_j}{\partial x_i} - \frac{2}{3} \delta_{ij} \frac{\partial u_k}{\partial x_k} \right) \frac{\partial u_i}{\partial x_j} \\ &= 2 \left[ \left( \frac{\partial u}{\partial x} \right)^2 + \left( \frac{\partial v}{\partial y} \right)^2 \right] + \left( \frac{\partial v}{\partial x} + \frac{\partial u}{\partial y} \right)^2 - \frac{2}{3} \left( \frac{\partial u}{\partial x} + \frac{\partial v}{\partial y} \right)^2 \end{aligned} \quad (23)$$

Using the same transformation techniques as in the discussion previously, the mean strain rate squared is transformed from  $(x,y)$  to  $(\xi,\eta)$  as follows:

$$\begin{aligned}
 S = & \frac{2}{J^2} [(y_\eta \frac{\partial u}{\partial \xi} - y_\xi \frac{\partial u}{\partial \eta})^2 + (-x_\eta \frac{\partial v}{\partial \xi} + x_\xi \frac{\partial v}{\partial \eta})^2] \\
 & + \frac{1}{J^2} (y_\eta \frac{\partial v}{\partial \xi} - y_\xi \frac{\partial v}{\partial \eta} - x_\eta \frac{\partial u}{\partial \xi} + x_\xi \frac{\partial u}{\partial \eta})^2 \\
 & - \frac{2}{3J^2} (y_\eta \frac{\partial u}{\partial \xi} - y_\xi \frac{\partial u}{\partial \eta} - x_\eta \frac{\partial v}{\partial \xi} + x_\xi \frac{\partial v}{\partial \eta})^2
 \end{aligned} \tag{24}$$

As discussed in reference 2, the nonlinear renormalized viscosity equation can be written in a cubic equation form:

$$v^3 - vSL_f^4 + (C_c - 1)v_0^3 = 0 \tag{25}$$

Kirtley [Ref. 4] showed the locus of possible allowable roots. If the maximum value of  $v$  is chosen as the proper root, a jump discontinuity in the distribution of  $v$  is yielded. A quartic equation transformed from equation (25) was used by Lund [Ref. 3], as follows:

$$v^4 - vv_0^3 - H(\tau'^2 L_f^4 - vC_c v_0^3) = 0 \tag{26}$$

where

$$\tau' = vS^{\frac{1}{2}} \tag{27}$$

and a preferable length scale proposed by Kirtley [Ref. 4] is the following:

$$L_f = C_\mu \delta \tanh\left(\frac{\kappa n}{C_\mu \delta}\right) \quad (28)$$

with  $C_\mu = 0.0845$ ,  $\kappa = 0.372$ , and  $n$  is the normal distance from the boundary, and  $\delta$  is the thickness of the boundary layer. An approximation of  $\delta$ , was suggested by Stock and Haase [Ref.11], as follows:

$$\delta = 1.936 y_{\max} \quad (29)$$

where  $y_{\max}$  is obtained from the Baldwin-Lomax turbulence model. The length scale  $L_f$  in the wake region of turbomachinery flows is determined from a correlation derived by Raj and Lakshminarayana [Ref.12] as follows:

$$L_f = \min(\kappa s, C_w b) \quad (30)$$

where

$$b = \delta_0 + c C_d^{\frac{1}{2}} 1.35 \left(\frac{s}{c} + 0.02\right)^{0.58} \quad (31)$$

and  $\delta_0$  is the average of the pressure-side and suction-side boundary layer thicknesses at the trailing edge,  $c$  is the chord, and  $C_w$ , the Gaussian constant for the wake behind a circular cylinder, is equal to 0.169. The equations above are the only empiricism in the RNG model.

Thus, the viscosity on every grid point in the flow field can be calculated from the solution of the quartic

equation as follows. First, an initial guess of the turbulent eddy viscosity is set equal to zero, before the flow solver starts its time marching iterative procedure. The algorithm for the RNG turbulence model is then as follows:

1. Calculate the boundary layer thickness, mixing length, and mean strain rate on every grid point.
2. Calculate the shear stress to density ratio based on the effective eddy viscosity at the  $n$  time step.
3. Evaluate the Heaviside function.
4. Apply Newton's method to solve the quartic equation for the effective eddy viscosity. There are two possibilities:
  - a. If the argument in the Heaviside function is positive, use that value for the Heaviside function.
  - b. If the argument in the Heaviside function is negative, then set the Heaviside function to zero.
5. Update the eddy viscosity and return to step 3, until the solution finally converges.
6. The converged solution is the effective eddy viscosity at the  $n+1$  time step.
7. Finally reevaluate the Heaviside function again and
  - a. if  $H > 0$ , the  $n+1$  time step effective eddy viscosity is used.

b. if  $H < 0$ , the  $n+1$  time step effective eddy viscosity is set equal to the laminar viscosity. This means the turbulent eddy viscosity equals zero.

8. A turbulent eddy viscosity-to-dynamic viscosity ratio is then calculated for RVCQ3D.

9. Return to main program.

After the RNG turbulence subroutine calculates the turbulent eddy viscosity, the value is stored in an array and becomes the initial guess for the next iteration calculation. The calculation direction is from the leading edge toward the trailing edge and then on through the wake. This was done so that the rate of growth of the boundary layer could be monitored.

The RNG model mimics the transition from laminar to turbulent flow within a boundary layer. As the Heaviside function suppresses deviations from laminar viscosity until the length scale and mean strain grows to values above the  $C_t$  cutoff. The same result occurs within the turbulent-to-laminar transition region. Thus the RNG model should be able to capture the viscous sublayer without any near-wall damping, while the Baldwin-Lomax model requires the addition of a damping term to describe the near-wall behavior.

### III. SOLUTION METHOD

#### A. GRID GENERATION

A transformation was used to transform a non-rectangular grid in the physical plane into a rectangular uniformly-spaced grid in the computational plane.

Two-dimensional body-fitted grids were generated using the GRAPE code (GRids about Airfoils using Poisson's Equation). This code was written by Sorenson, primarily for isolated airfoils [Ref.13]. A modified GRAPE code [Ref.14] was used for the generation of periodic C-type grids for turbomachinery cascades. For viscous flow, the grids are typically finer normal to the blade than in the streamwise direction.

The locations of the intersection of grid lines with the inner and outer boundaries were controlled to give minimum shear in these regions. It is desired to have near-wall normal grid lines at the blade surfaces. However, because of the large amount of turning, normal grid lines could not be generated over the entire blade surface and still maintain the grid line periodicity on the outer boundary. The presence of the sheared grid lines did not appear to adversely effect the flow solutions.

## B. NUMERICAL SCHEME

The code employs an explicit, finite-difference, multi-stage, Runge-Kutta algorithm. The governing equations are discretized using a node-centered finite-difference scheme [Ref. 15 and Ref. 16]:

$$q_1 = \hat{F}_0^{(n)} - \alpha_1 \Delta t R(\hat{F}_0^{(n)}) \quad (32)$$

$$q_2 = \hat{F}_0^{(n)} - \alpha_2 \Delta t R(q_1) \quad (33)$$

$$q_3 = \hat{F}_0^{(n)} - \alpha_3 \Delta t R(q_2) \quad (34)$$

$$q_4 = \hat{F}_0^{(n)} - \Delta t R(q_3) \quad (35)$$

$$\hat{F}_0^{(n+1)} = q_4 \quad (36)$$

where  $\alpha_3 = 1/2$ ,  $\alpha_2 = 1/3$ ,  $\alpha_1 = 1/4$ , and

$$R = \frac{1}{2} [ (\hat{F}_{1\ i+1}^j - \hat{F}_{1\ i-1}^j) + (\hat{F}_{2\ i}^{j+1} - \hat{F}_{2\ i}^{j-1}) - \frac{1}{Re} (\hat{F}_{4\ i}^{j+1} - \hat{F}_{4\ i}^{j-1}) ] \quad (37)$$

Second- and fourth-order artificial-dissipation terms are added to stabilize the scheme. A spatially varying time step and implicit residual smoothing are used to accelerate convergence.

### C. BOUNDARY CONDITIONS

At the cascade inlet, absolute total temperature  $T_0$ , absolute total pressure  $P_0$ , relative velocity, and relative flow angle are specified as constants. For subsonic flows, the inlet conditions are updated at each iteration by extrapolating the upstream-running Riemann invariant  $R^-$  based on the absolute total velocity  $Q$  to the inlet, where

$$R^- = Q - \frac{2c}{\gamma-1} \quad (38)$$

Then, using the known total temperature  $T_0$  and the isentropic relations, the total velocity magnitude is given by

$$Q = \frac{(\gamma-1)R^- + \sqrt{4(\gamma+1)C_p T_0 - 2(\gamma-1)(R^-)^2}}{(\gamma+1)} \quad (39)$$

Individual velocity components are found from trigonometric relations by keeping the tangential velocity component fixed. Pressure and density are found from isentropic relations. On the blade surfaces, for viscous flow, the no-slip velocity boundary condition is used. The surface pressures are computed using the normal momentum equation, namely

$$(\eta_x \xi_x + \eta_y \xi_y) p_\xi + (\eta_x^2 + \eta_y^2) p_\eta = -\rho U (\eta_x u_\xi + \eta_y v_\xi) \quad (40)$$

where  $U = V = 0$  on the surface for viscous flow.

Surface densities are found from surface pressures and a specified wall temperature. Both the Baldwin-Lomax and RNG

turbulence models incorporated Sutherland's viscosity law to calculate the dynamic viscosity.

The exit static pressure is determined by specifying the exit static-to-inlet total pressure ratio. All other flow quantities are extrapolated at the exit plane. Periodicity is enforced on the "C" grid by using a pseudo-point along the periodic boundaries on which corresponding pitchwise variables are located.

#### IV. RESULTS AND DISCUSSION

Two blade profiles that were part of the full-annular ring of 36 blades, with C-type gridding over the computational domain, are shown in Figure 1. The chord length of the actual vane was 55.54 mm long. The geometry of a full 250 X 60 mesh size (150 grid lines around the airfoil, 50 grid lines on each side of the center line in the wake region) is shown in Figure A1 in Appendix A.

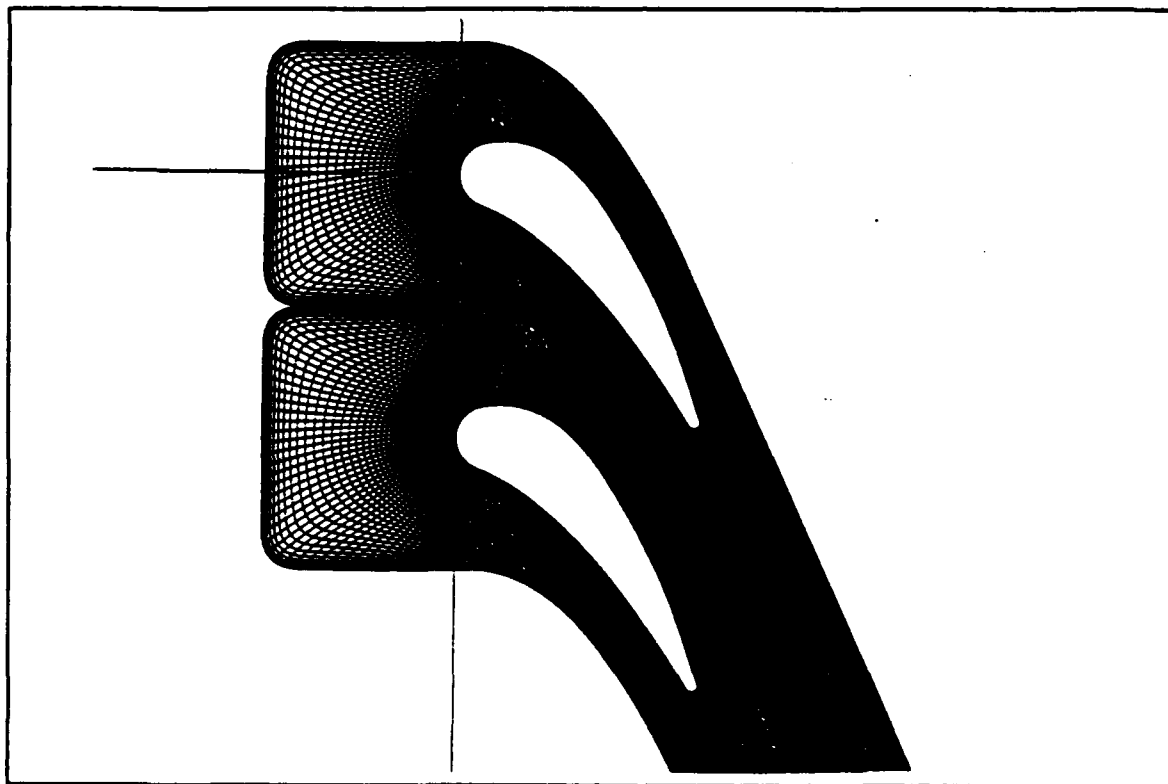


Figure 1 The geometry of Goldman's annular cascade

The experimental investigation of this cascade [Ref. 7] was conducted with the hub-static to inlet-total pressure ratio maintained at a value of 0.65. This corresponds to a mean-radius, ideal, exit, critical velocity ratio of 0.78. In Chima [Ref. 17], a boundary condition and initial condition input file for the RVCQ3D code was provided. The computational results in the next section were calculated with an exit-static pressure to inlet-total pressure ratio of 0.685. The data of streamtube variation (Appendix A.) were provided by Goldman [Ref. 18].

## A. STREAMTUBE VARIATION AND GRID RESOLUTION

### 1. STREAMTUBE VARIATION

The predicted blade surface pressure distribution, without streamtube variation, did not agree well with Goldman's experimental data [Ref. 7]. In order to obtain a good baseline solution, with the Baldwin-Lomax turbulence model, streamtube variation based on Goldman's [Ref. 18] throughflow calculations was introduced.

The effect of streamtube variation in the convergence rate is shown in Figure 2. The application of a varying

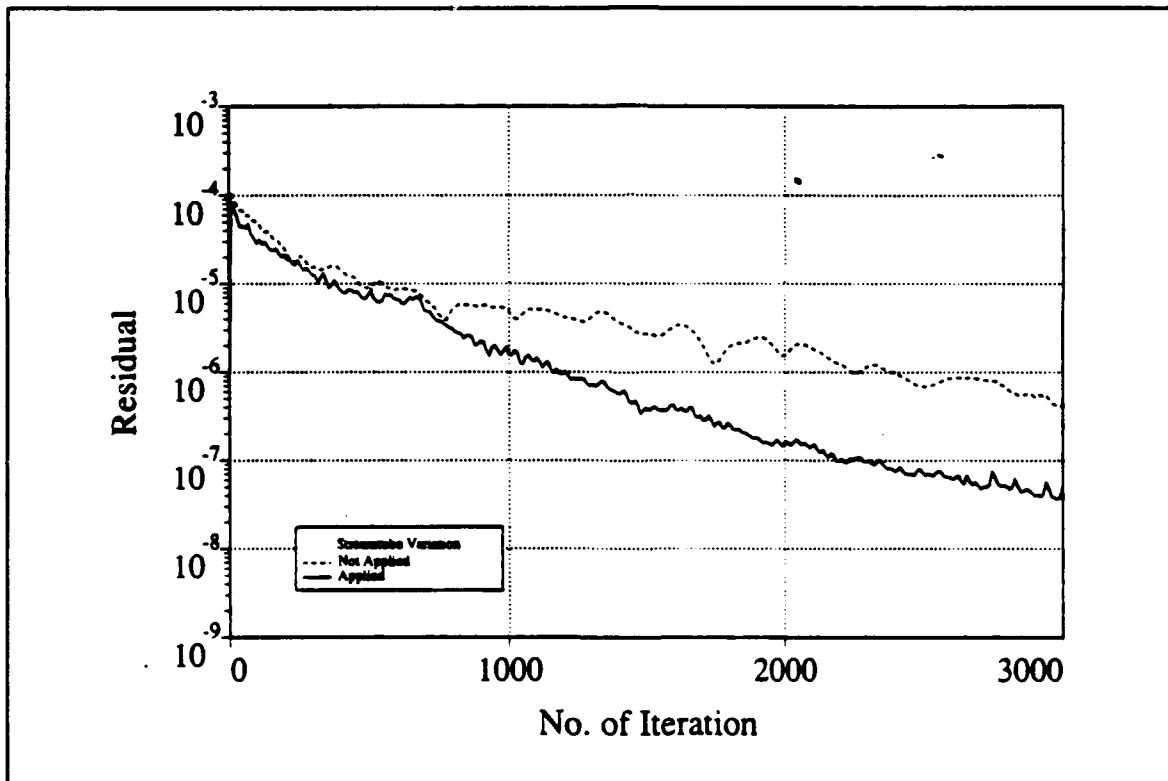
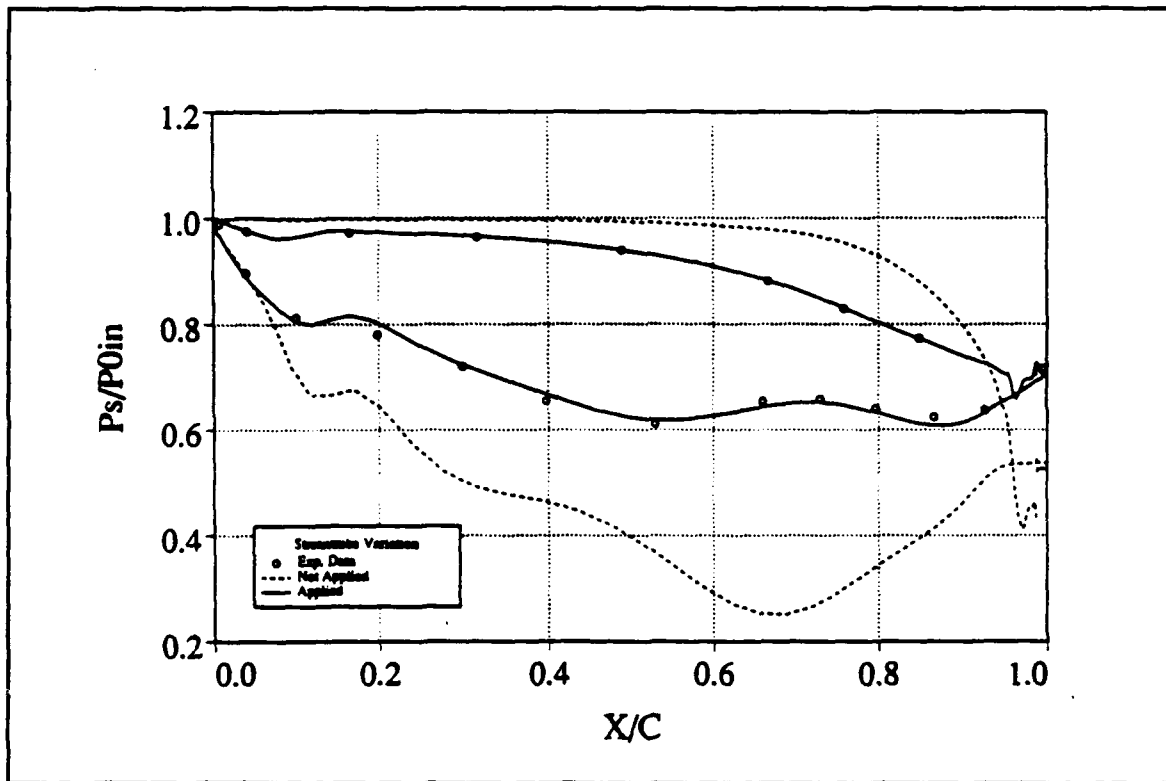


Figure 2 Streamtube variation effects on convergence history

streamtube resulted in better convergence as it maintained a near constant convergence rate, particularly after 1000 iterations, and finally gave an order of magnitude improvement on the convergence after 3000 iterations.

Streamtube variation had a significant effect on the prediction of the blade surface pressure distribution as can be seen in Figure 3.



**Figure 3** Streamtube variation effects on pressure ratio distribution

Constant streamtube thickness and radial location versus axial distance through the cascade resulted in a poor prediction of static pressure. Not only were the levels of static pressure quite different, but the shape of the suction

side pressure distribution was also not predicted properly.

Finally the wake distribution predicted with and without streamtube variation is shown in Figure 4. Once again a significant improvement on not only the level of velocity in the wake but the shape of the wake profile is obtained with streamtube variation. The same streamtube variation study using a grid size of 97 X 31 is shown in Appendix B, Figures B1, B2, and B3.

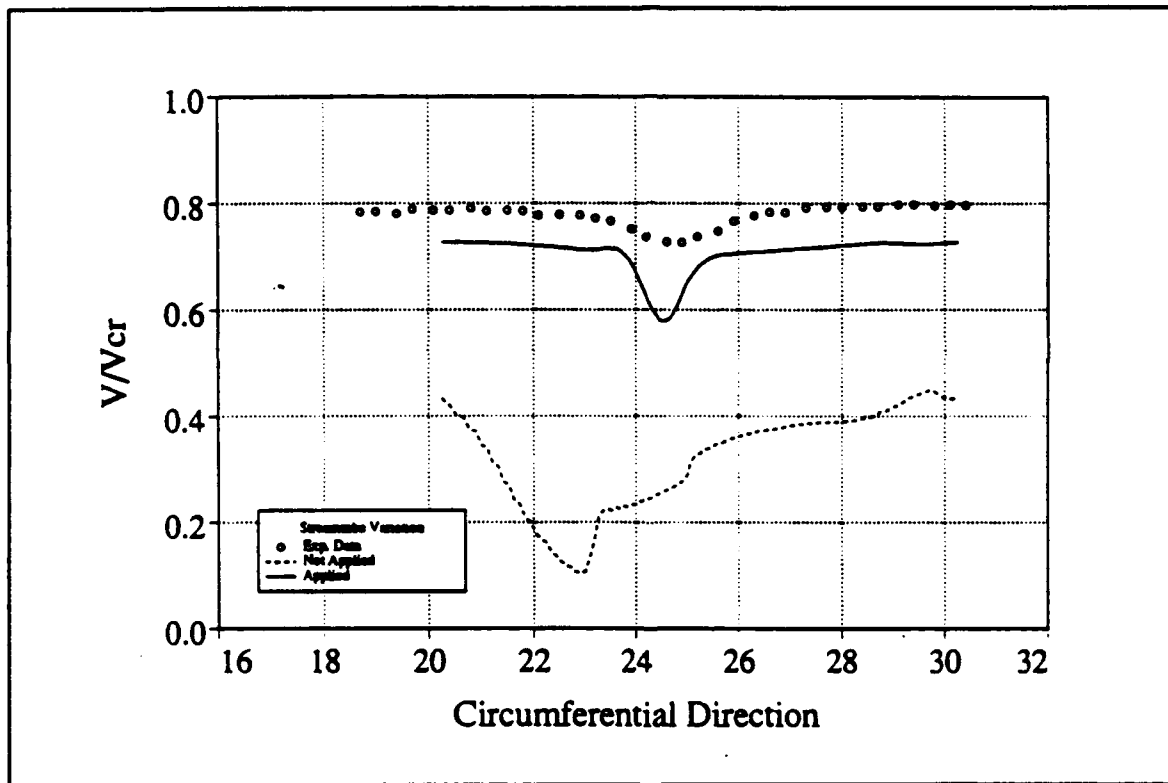


Figure 4 Streamtube variation effects on wake velocity ratio distribution

## 2. GRID RESOLUTION

In order to determine the best grid resolution for the blade-to-blade viscous flow analysis, the influence of the grid size on the flow characteristics was studied. The solutions of three different grids, 97 X 31, 200 X 31, and 250 X 60, were compared for the analysis of Goldman's annular turbine cascade.

All of the three different sized grids were run to 3000 iterations with the same boundary conditions and a Courant number of 4.0. The convergence history is shown in Figure 5.

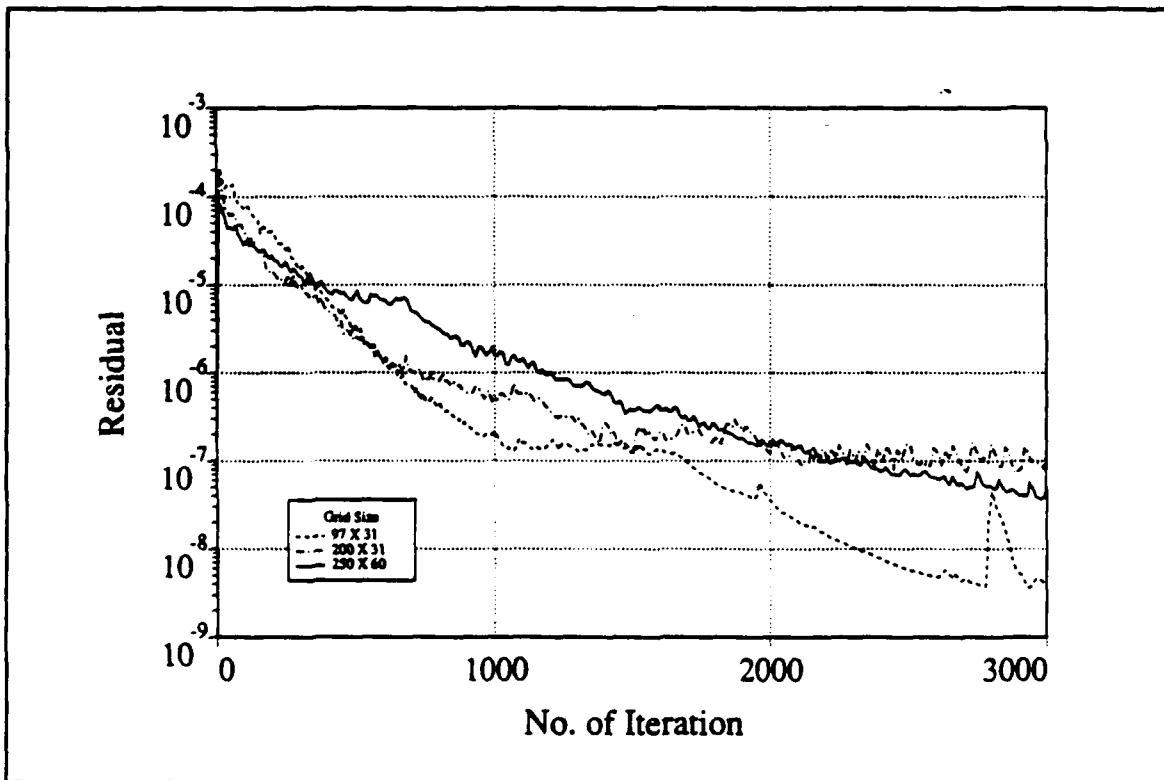
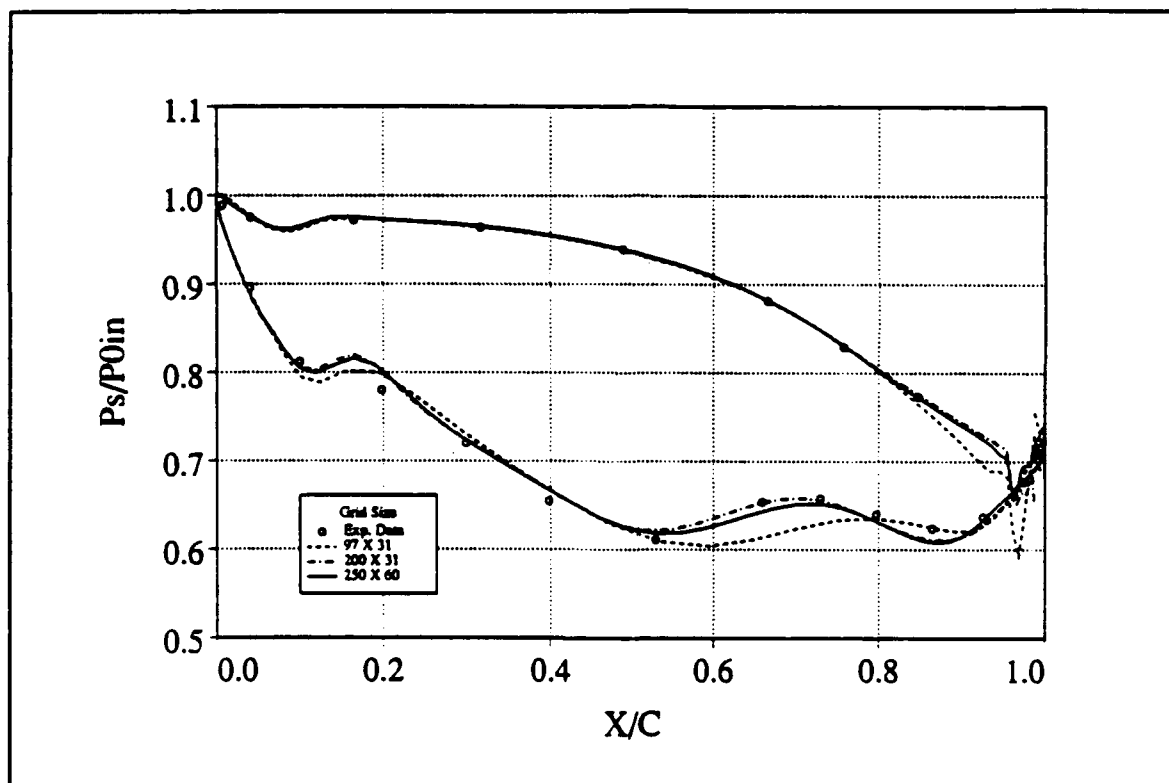


Figure 5 Grid resolution effect on convergence history

Initially the convergence rate of the coarse grid is better than the two finer grids, however this shows signs of instability in the latter part of the convergence history. Both the fine grids (200 X 31 and 250 X 60) showed similar convergence histories and they both achieved approximately three orders of magnitude convergence after 3000 iterations.

The effect of grid resolution on the prediction of the midspan blade surface pressure distribution is shown in Figure 6.



**Figure 6** Grid resolution effect on blade surface static pressure to inlet total pressure ratio

Grid refinement from 97 X 31 to 200 X 31 shows an improvement in blade surface pressure distribution when compared with experiment, particularly on the suction side of the blade. Further refinement from the 200 X 31 to 250 X 60 showed little improvement in the pressure distribution, hence the solution with this size grid was felt to be grid independent and subsequently used throughout the investigation. The 250 X 60 grid solution also gave the best resolution at the trailing edge as the "overshoot" in  $P_1/P_{0\infty}$  was the least for this test case.

An investigation of the grid resolution was also performed on the wake profile prediction. At the 153.2 percent axial chord position, a comparison of experimental data with the prediction of local velocity to critical velocity ratio is shown in Figure 7.

The coarse grid clearly produced a wake profile which was highly grid dependent, as the profile was not smooth at the wake center line. Grid refinement improved this as well as the prediction of the free-stream velocity. However, the pressure side profile shows an overshoot which is not evident in the experimental data. The 250 X 60 grid produced the best shape for the wake profile, but the deficit in the wake is overpredicted and the wake diffusion or growth is underpredicted. The discrepancy in the free-stream velocity is

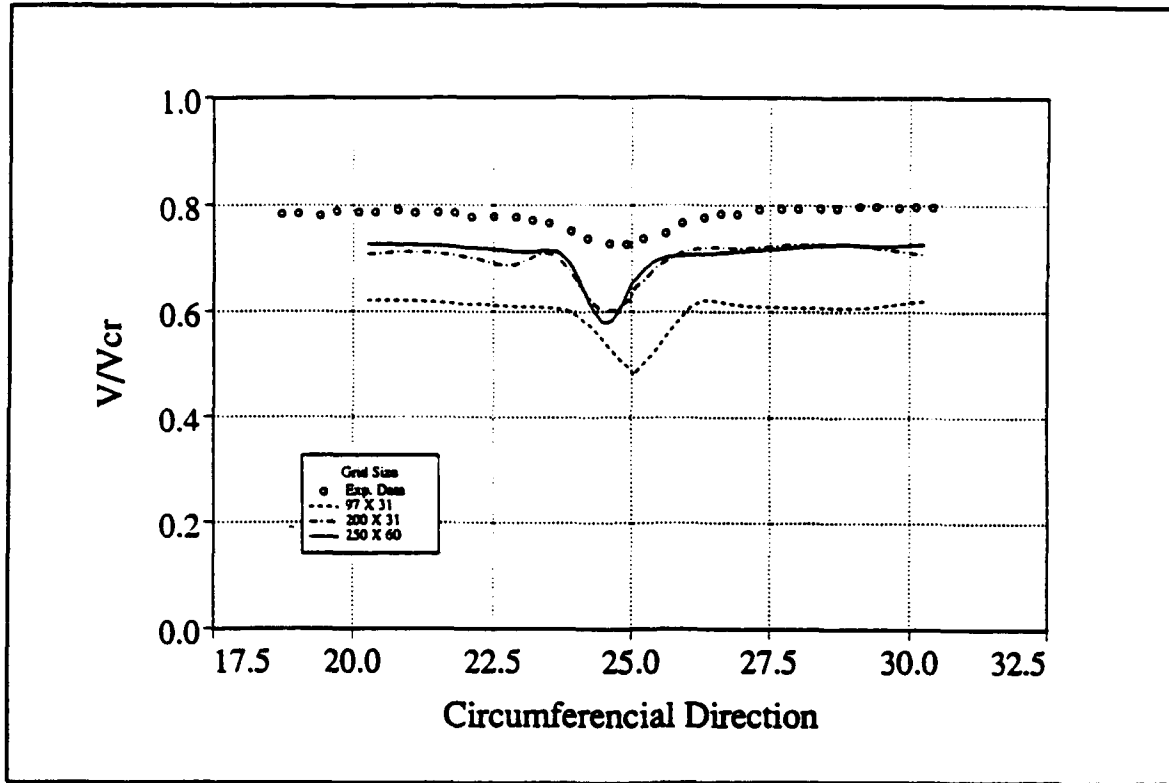


**Figure 7** Grid resolution effect on velocity ratio at 153.2 axial chord position

attributed to the inability of the streamtube contraction to account for the three-dimensional effects in the annular cascade.

## B. B-L MODEL AND RNG MODEL

In order to test the performance of the RNG-based turbulence model in the RVCQ3D code, identical test cases were run with the Baldwin-Lomax and RNG turbulence models. Also a fully laminar flow calculation was included for comparison. Unfortunately, the RNG model did not give a converged solution after 3000 iterations. In Figure 8, the convergence history shows that the RNG turbulence model was just calculating the laminar flow condition.

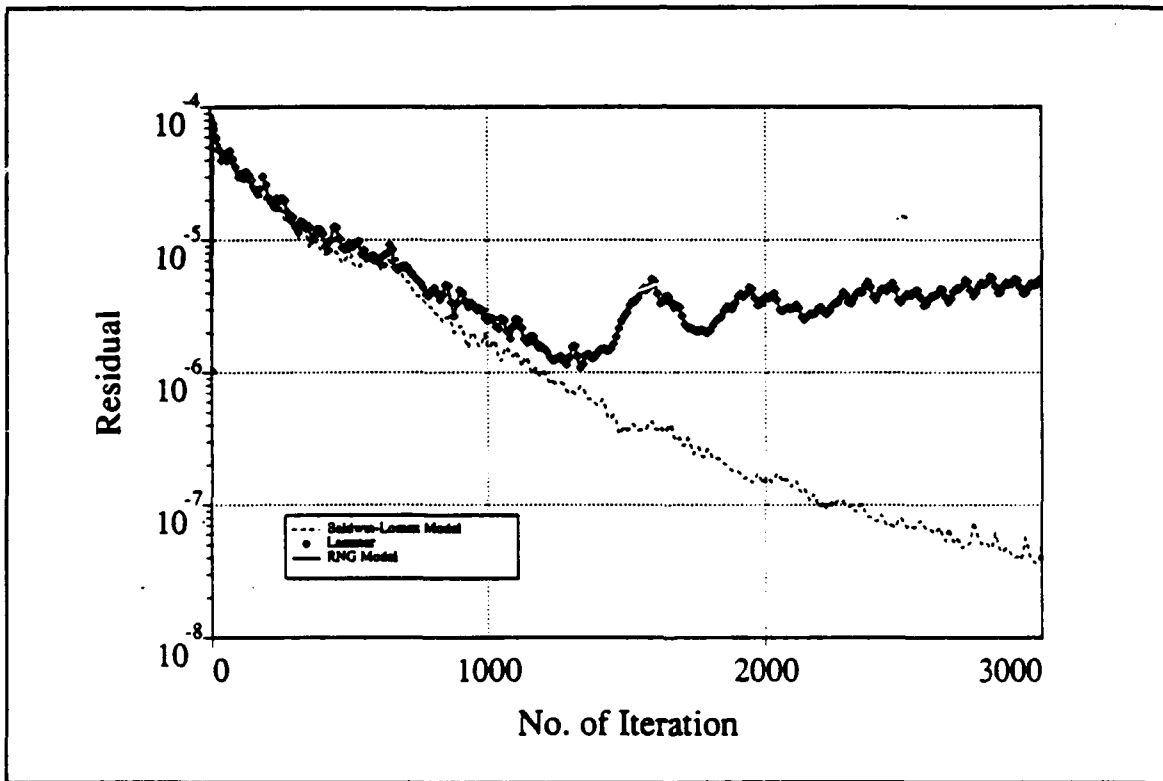


Figure 8 Turbulence model effect on convergence history

The flow velocity vector around the trailing edge for the Baldwin-Lomax turbulence model and RNG turbulence model are shown in Figures 9 and 10, respectively. The velocity vector plot of the Baldwin-Lomax model solution shows a near-symmetric double recirculation region aft of the trailing edge in the turbulent wake. The extent of this recirculation region is approximately 1.2 trailing edge thicknesses in the streamwise direction; however, the velocity vector plot of the RNG model solution was asymmetric. The suction-side boundary layer separated because it was still laminar near the trailing edge and this resulted in the large recirculation region on the suction side which extended aft of the trailing edge to approximately 2.5 trailing edge thicknesses downstream of the blade. Separation started from about  $1/5$  of the chord length from the trailing edge on the suction side surface. This is also the evident in the laminar flow test case.

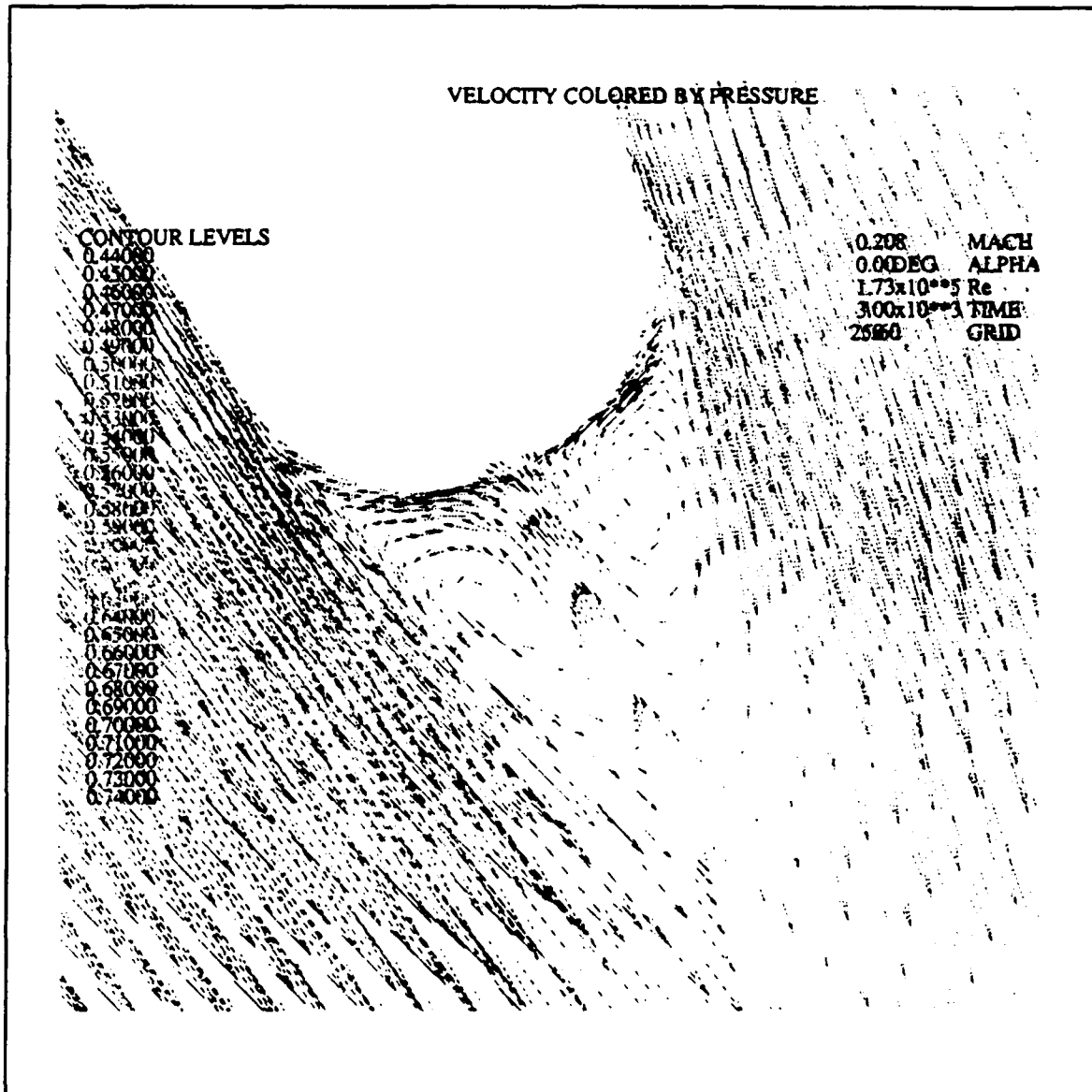


Figure 9 Velocity vector plot of B-L model

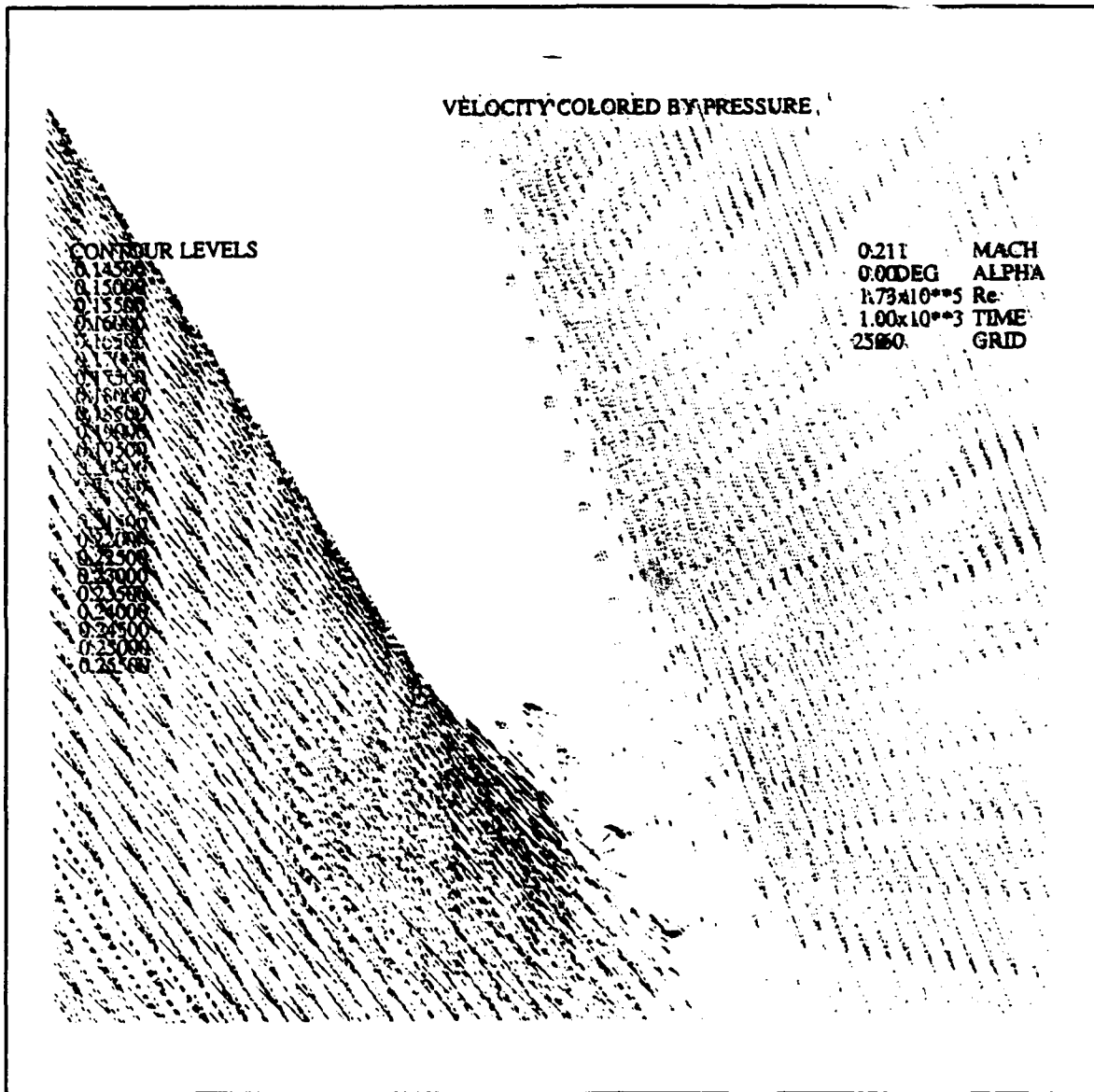


Figure 10 Velocity vector plot of RNG model

## 1. BLADE SURFACE PRESSURE DISTRIBUTION

All of the following comparisons between the B-L and RNG turbulence model are made for conditions after 1000 iterations, as this is almost at the best convergence of the RNG model. However the B-L results could be substantially improved if allowed to continue to full convergence beyond 3000 iterations. In Figure 11, the prediction of the blade surface static pressure to inlet total pressure ratio is shown.

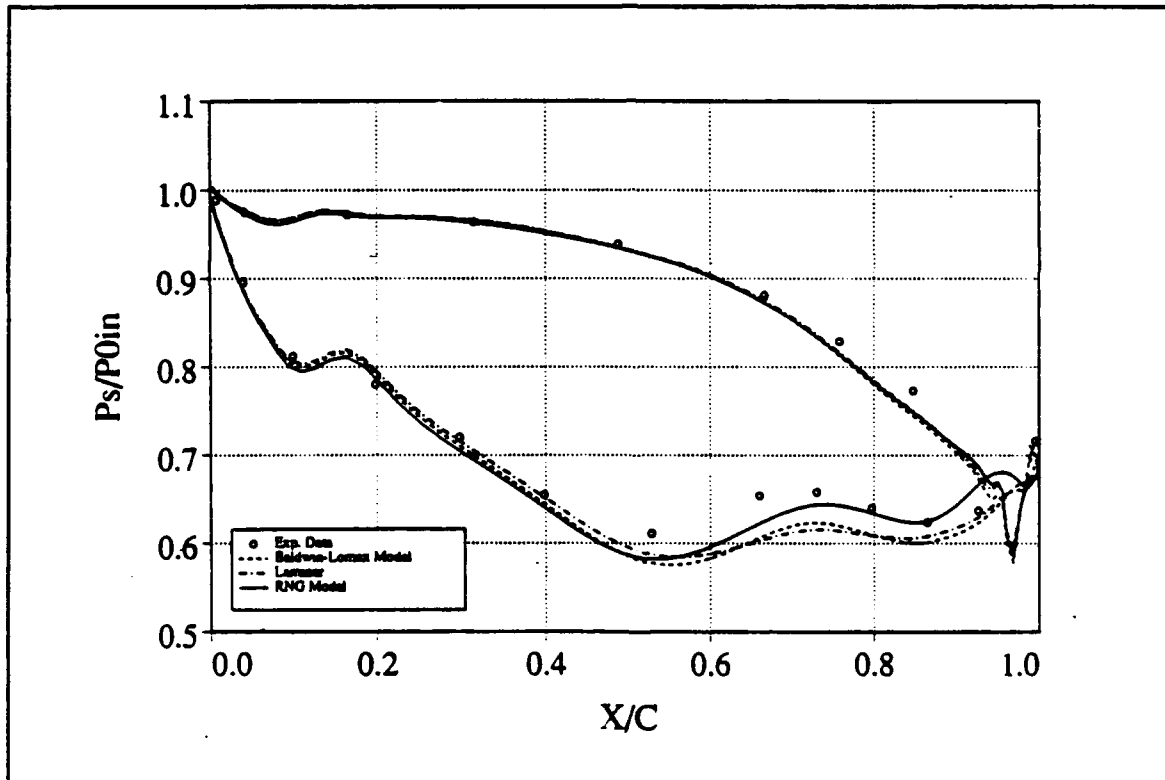
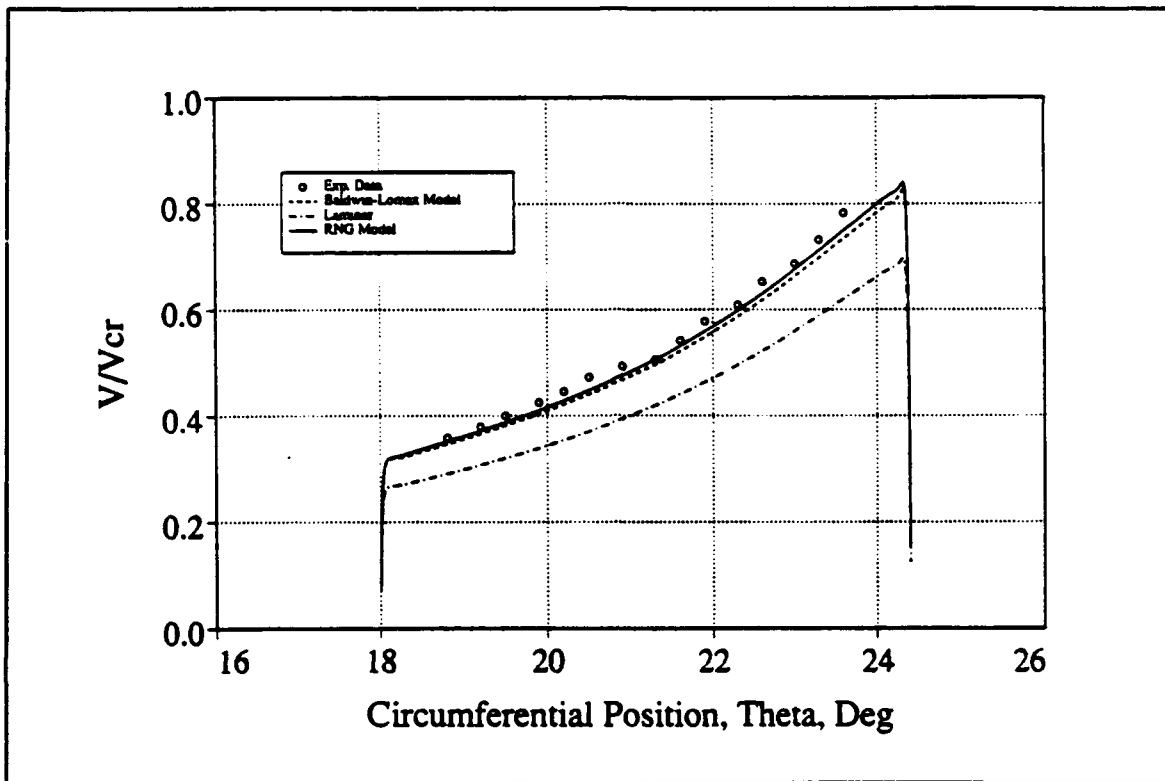


Figure 11 Turbulence model comparison of blade surface static pressure prediction

Figure 8 showed that the RNG turbulence model gave a convergence history similar to the laminar flow solution, and Figure 10 showed the laminar flow behavior of the RNG model at the trailing edge. But Figure 11 shows that the RNG turbulence model produced a different pressure distribution to the laminar flow case. On examination of the results over the whole computational domain, the turbulent eddy viscosity around the airfoil out to the freestream, was found to be equal to zero. However the eddy viscosity was not equal to zero in the wake region. Since the mixing length formulation is modified in the wake region, and is different from the calculation in the region around the airfoil, this would explain why the RNG turbulence solution was not the same as the laminar flow solution. And because of this, turbulent flow was actually calculated in the wake region. The RNG solution gave a better prediction of the pressure distribution, particularly on the suction surface of the blade.

In Figure 13, the flow velocity to critical velocity ratio in the circumferential direction at 50 percent chord from the pressure-side to suction-side is shown.



**Figure 13** Turbulence model comparison of velocity-to-critical velocity ratio at 50 percent chord

The Baldwin-Lomax and RNG turbulence model solutions at the 50 percent chord position are comparable.

## 2. MIDCHORD FLOWFIELD COMPARISON

In Figure 12, at the 50 percent chord position, the blade-to-blade distribution of  $C_p$  from pressure-side to suction-side is shown. Here, all three test cases show comparable results. Notice that the RNG turbulence model is slightly different from the other two test cases in the near suction-side region. This difference is likely to be the effect of the recirculation on the suction-side of the blade near to the trailing edge.

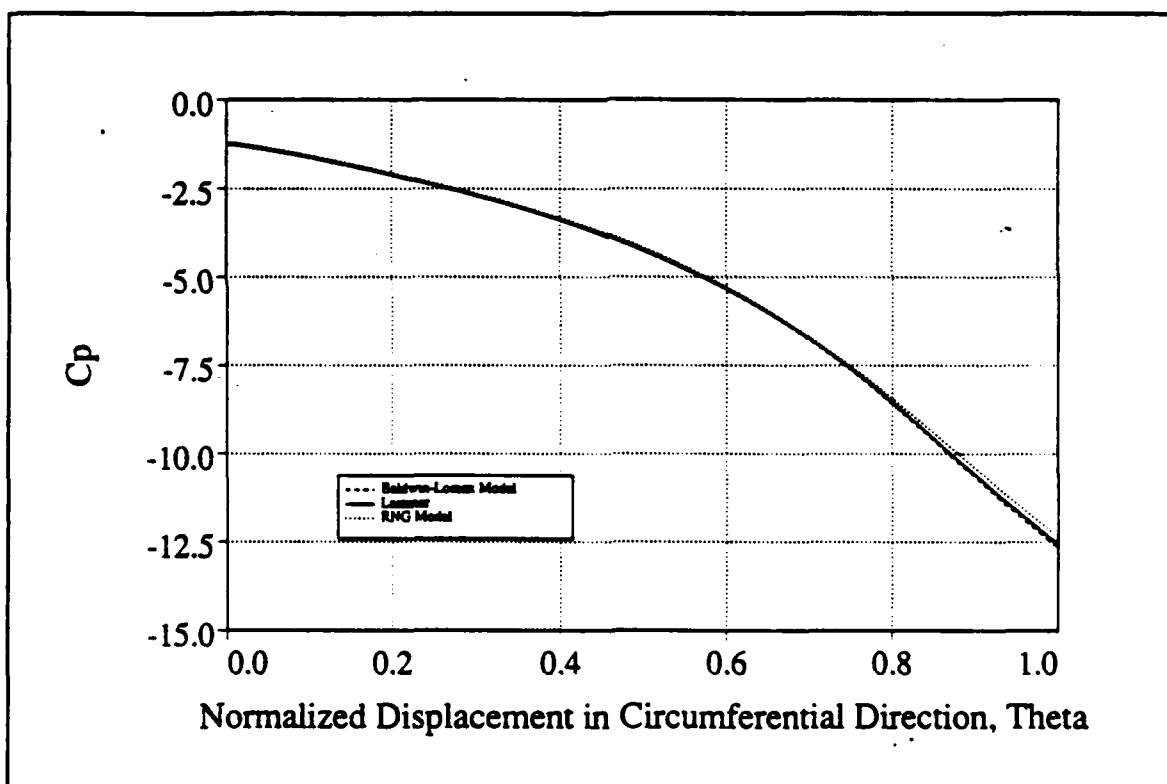


Figure 12 Turbulence model comparison of  $C_p$  prediction at 50 percent chord

For completeness, the predicted blade-to-blade flow angle distribution in the circumferential direction from the pressure-side to suction-side is compared to the experimentally measured data, and is shown in Figure 14.

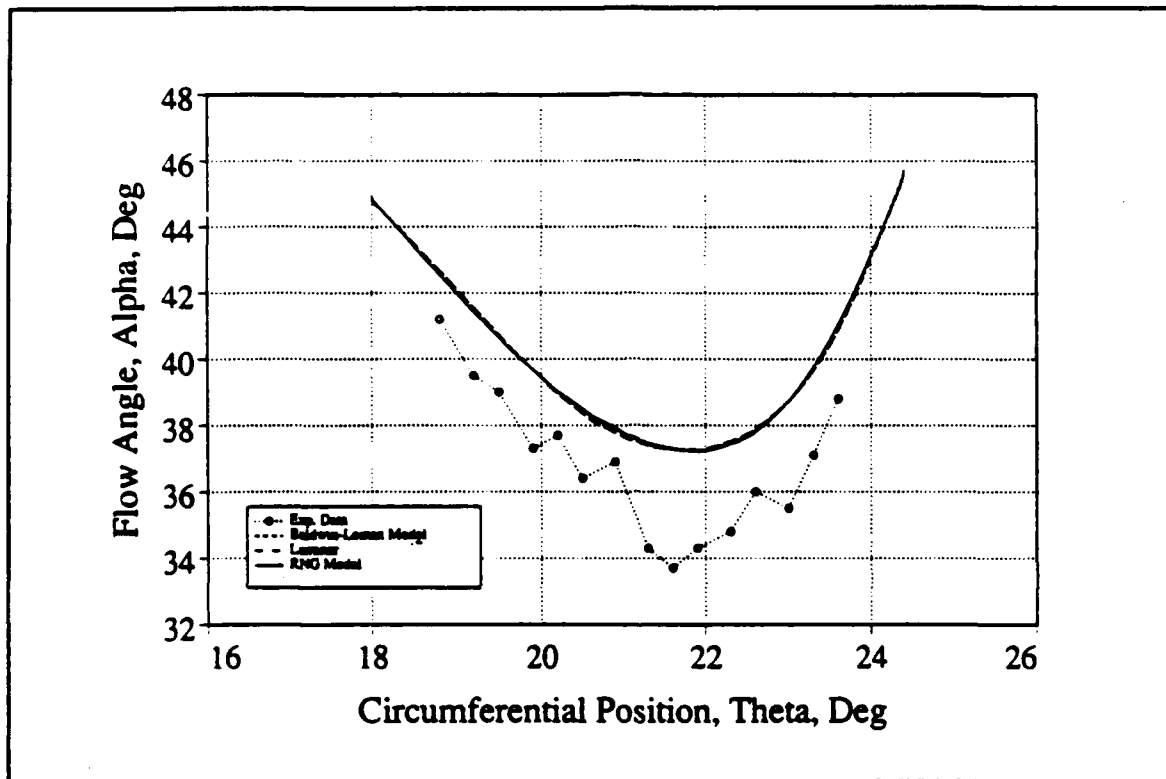
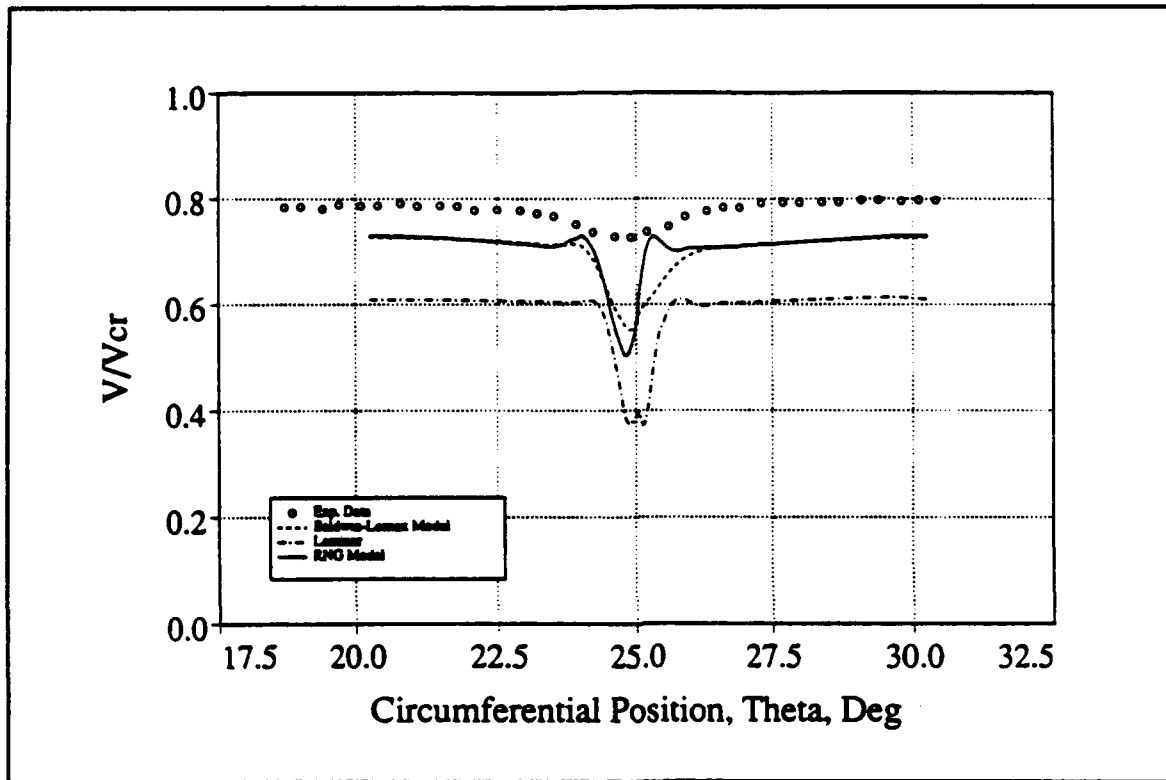


Figure 14 Flow angle distribution at 50 percent chord

### 3. WAKE PREDICTION

The wake prediction with the Baldwin-Lomax and RNG turbulence models and the laminar flow calculation, are shown in Figure 15.



**Figure 15** Turbulence model comparison of wake prediction, from pressure-side to suction-side

The Baldwin-Lomax and RNG turbulence models both give a good prediction of the freestream velocity magnitude, but the Baldwin-Lomax model gives the best wake center line position and the velocity deficit.

### C. DISCUSSION

As the RNG turbulence model case did not completely converge after a large number of iterations, two major parameters in the quartic equation which are inside the Heaviside function were investigated. These parameters were the mixing length and the shear stress. Since the RNG model only solved laminar flow during the initial 1000 time steps, this meant the Heaviside function inside the quartic equation was always negative.

The constant,  $C_e$ , in the Heaviside function was initially set equal to 200. In order to reduce the contribution of the negative term in the Heaviside-function calculation, the smallest value of  $C_e$ , 75, was used.

Figure 16 shows the comparison of the predicted mixing length for both the Baldwin-Lomax and RNG models. This is shown for the grid line 190, which is normal to the blade surface, close to the trailing edge (which is at line 200). This comparison is done at this location, because it was felt that the boundary layer should be fully turbulent at this station as predicted with the Baldwin-Lomax model. Transition was determined to take place at the 165 grid line, which is located at approximately 60 percent chord. Both models reach a maximum of  $L_t$  inside the boundary layer and these values are

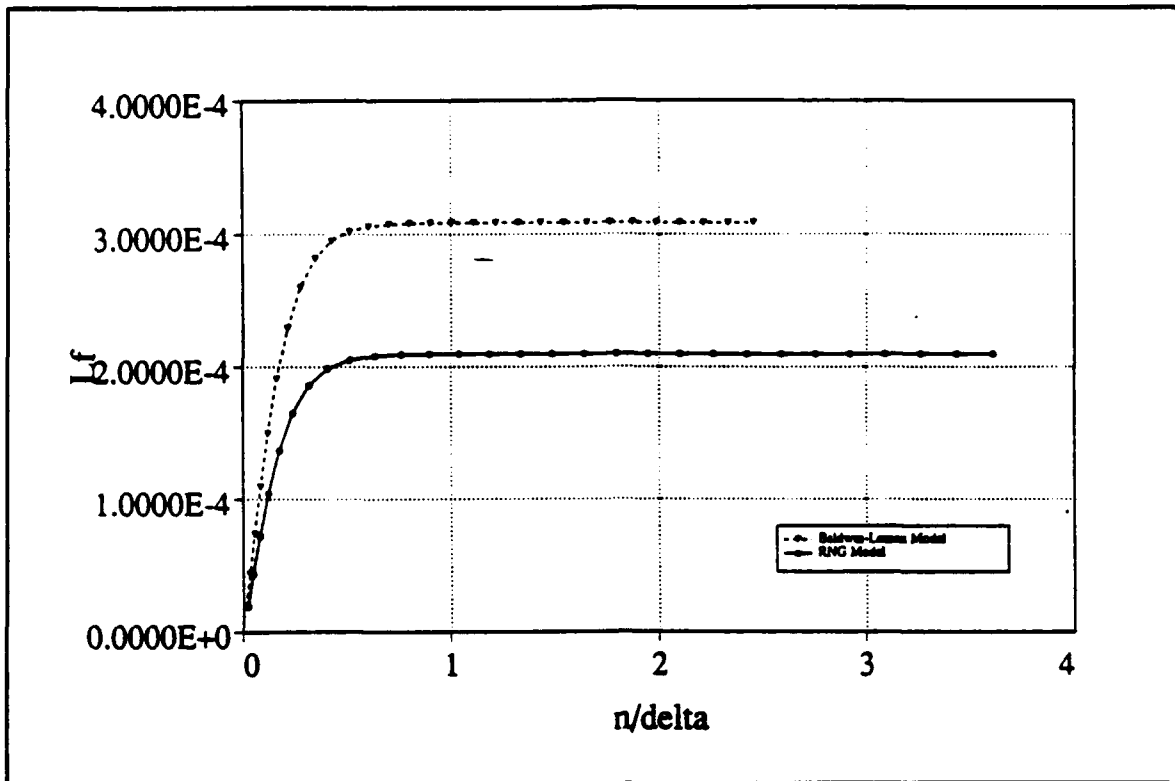


**Figure 16** Comparison of B-L and RNG mixing length distributions normal to the suction surface

within 30 percent of each other. If we assume that the Baldwin-Lomax model-derived mixing length is correct then the RNG model mixing length, which is based on the boundary layer thickness,  $\delta$ , seems to be correct.

In Figure 17, the shear stress distribution versus normal distance to boundary-layer thickness ratio is shown. Here an obvious discrepancy in the level of prediction of  $\tau$  is evident, which most probably resulted in the Heaviside function not going positive and therefore not initiating turbulent flow calculations.

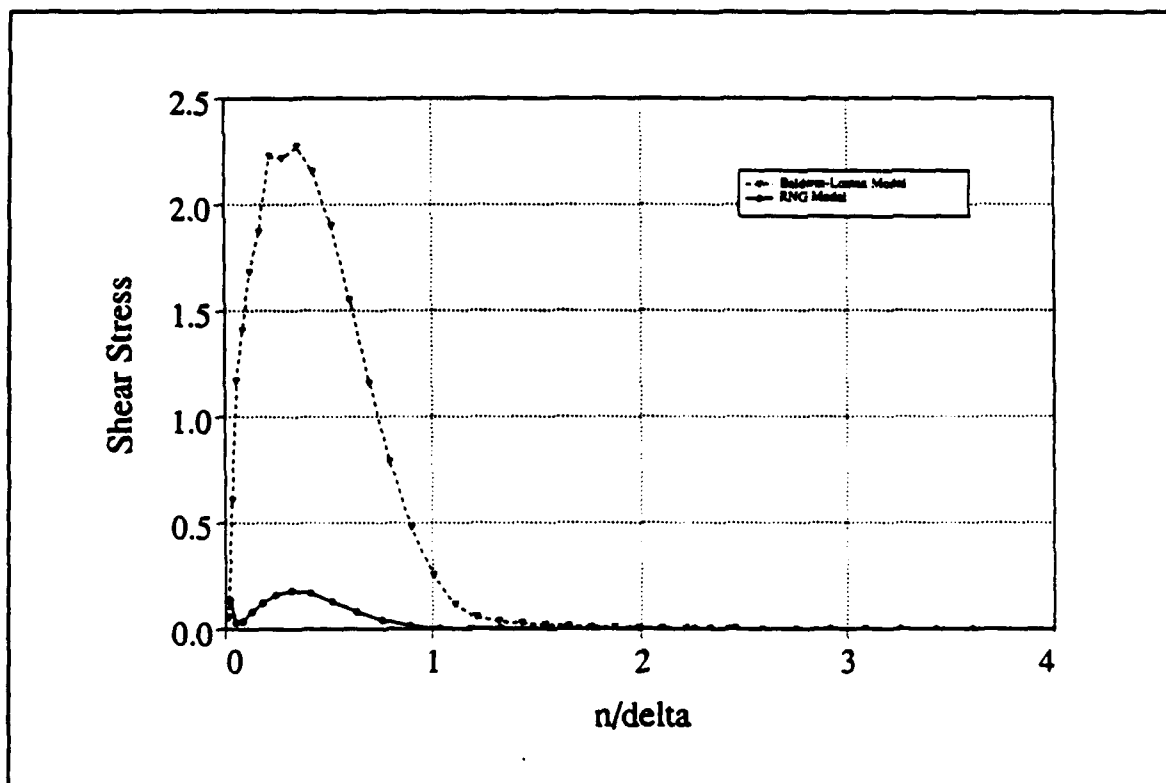


Figure 17 Comparison of B-L and RNG shear stress distributions normal to the suction surface

An extra check can be made on the derivation of the mean strain rate, equation (24). The vorticity calculated by the Baldwin-Lomax turbulence model at the wall, and the mean strain rate at the wall around the blade surface, are shown compared in Figure 18. They are in agreement everywhere except at a few points close to both leading edge and trailing edge.

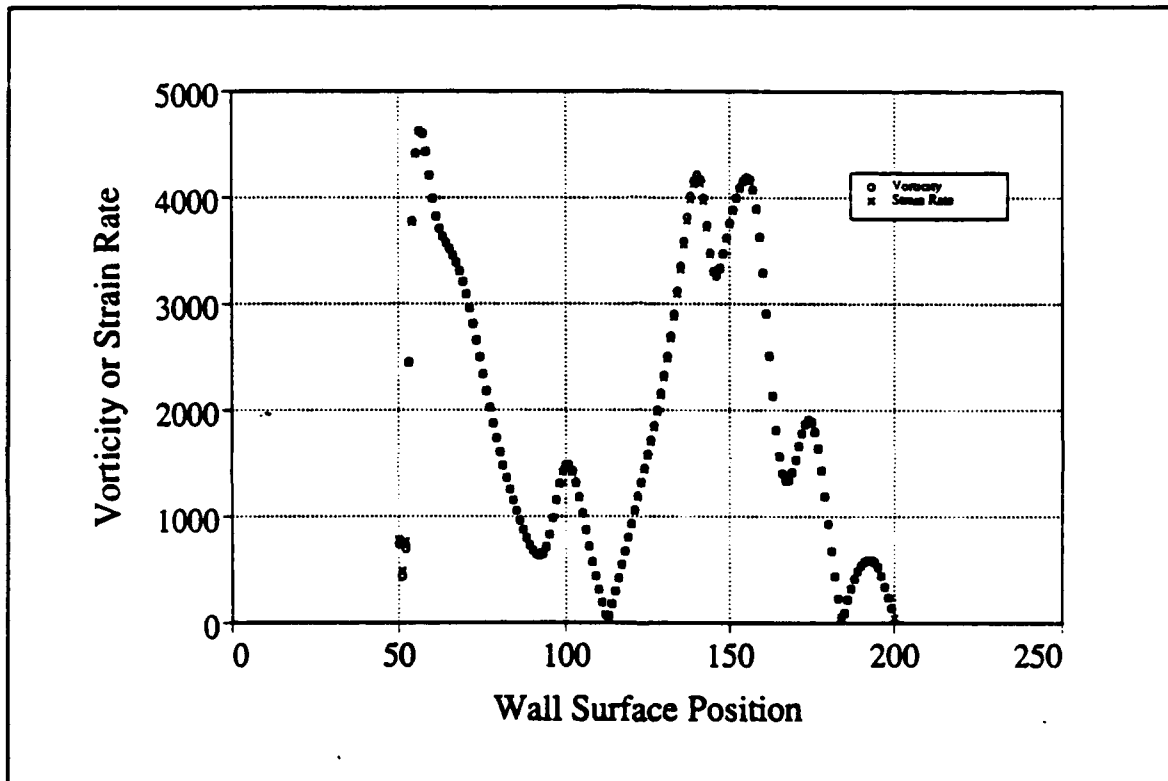
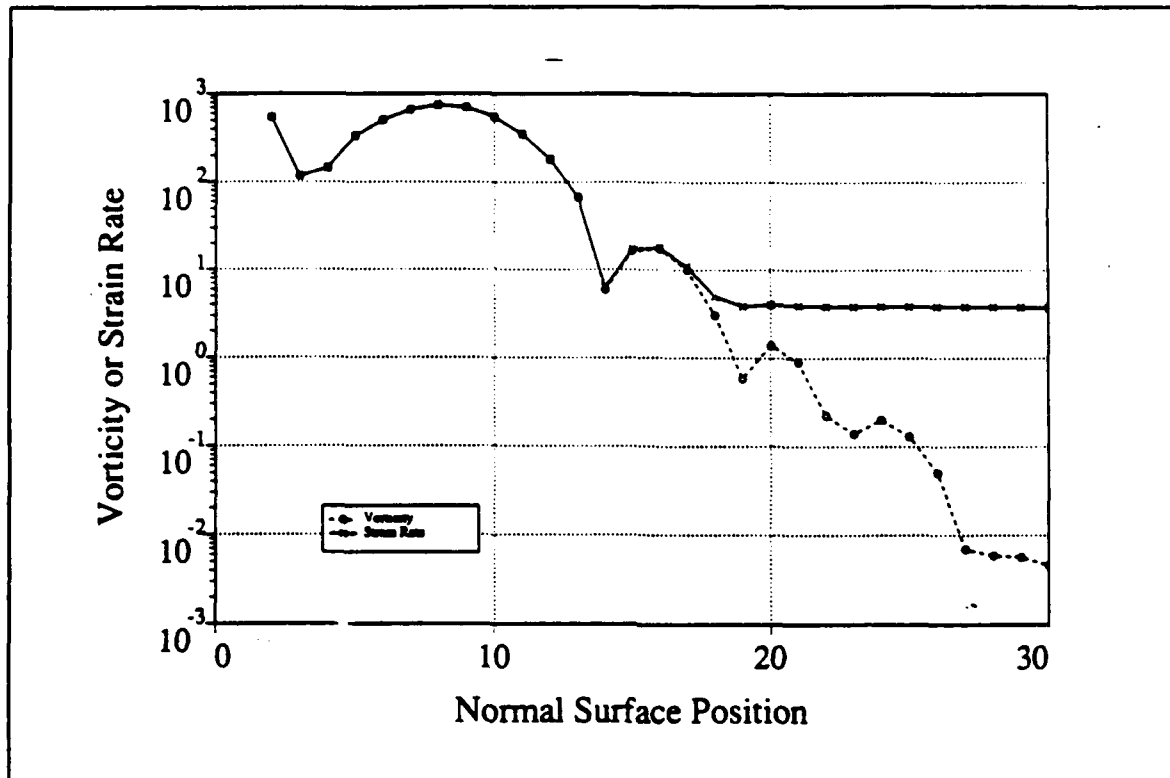


Figure 18 Shear strain and vorticity distribution on the blade surface

The same quantities plotted along the 190 grid line is shown in Figure 19. For the near-wall region, the first 15 grid points off the blade surface are identical.



**Figure 19** Shear strain rate and vorticity distribution normal to the suction surface

Since the values of computed vorticity and mean strain rate are exactly the same at the blade surface, this verifies that the derivation and coding of equation (24) are correct. As the vorticity at the wall is equal to the normal velocity gradient and the mean strain rate is also equal to this quantity.

## V. CONCLUSION

The annular turbine cascade flowfield calculation with the RVCQ3D code, which is based on the Baldwin-Lomax turbulence model, is grid dependent. Increasing the number of grid points around the body is a more efficient way to improve the solution than increasing the number of points normal to the body. A quasi-three-dimensional calculation which includes the streamtube variation information is strongly recommended, particular for this annular cascade test case.

Initial indications were that the RNG model showed similar convergence (a logical first check) to the Baldwin-Lomax turbulence model for the first 1000 iteration, after which the RNG model diverged. The divergence of the RNG model could be expected as the model is highly non-linear, and most probably less robust than the Baldwin-Lomax model. The comparison of the computed flowfield at 1000 iteration, showed that the Baldwin-Lomax model was overall better than the RNG model. However, upon further investigation it was determined that the RNG model only computed laminar flow over the blade surface and turbulent flow in the wake. As the RNG model did quite well in the wake region, it should be further investigated as a possible wake modification to the Baldwin-Lomax model.

The RNG model calculation was initiated by assuming laminar flow initially as described by Kirtley [Ref. 4], and

this resulted in the Heaviside function always being negative. Another method, which should be tried is to begin from the high-Reynolds number limit as proposed by Lund [Ref. 3] and use the RNG model to update the provisional eddy viscosity; i.e., begin with a positive Heaviside function.

## APPENDIX A DATA FOR GOLDMAN'S CASCADE

The complete 250 X 60 C-type grid for Goldman's cascade is shown in Figure A1. Data for the variation of the streamtube thickness through Goldman's cascade are given in Figure A2.

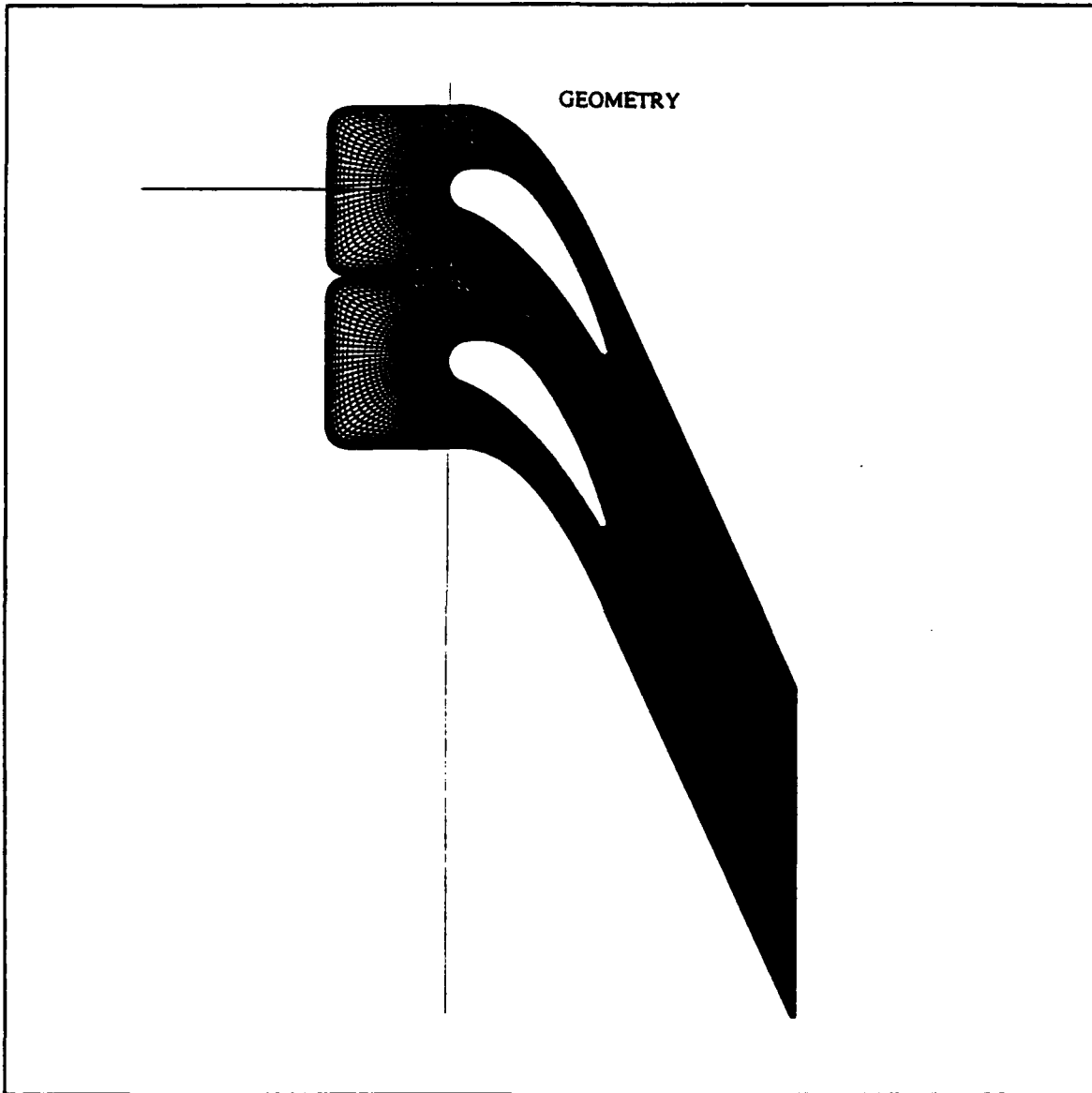


Figure A1 Geometry of C-type 250 X 60 grid

```

'ANNULAR TURBINE, TURBULENT'
&NL1 M=250,N=60,MTL=50,MIL=112 &end
&NL2 NSTG=4,IVTSTP=1,IBC=1,IEX=1,MAXTC=2000,AVISC2=0.,AVISC4=1.,
CFL=4.0,EPSCON=1.E-20,IRS=1,EPX=.30,EPN=.40 &END
&NL3 IRSTRT=0,IRVC=3,IRE=10,ICRNT=10000,ISIR=50000,IPIR=10000,
IXRM=0 &END
&NL4 PI=2116.0,TI=518.69,PRAT=0.685,WLE=235.4,ALLE=00.0,
ALTE=-67.0,RGAS=1716.48,CEPE=6007.68 &END
&NL5 ILT=2,DYVISI=3.99E-7,XSCL=1.0,PRNR=.70,TWALL=518.69,
CMUTM=0.0,JEDGE=30 &END
&NL6 OMEGA=0.0,NBLADE=36,NMN=36 &end
-0.125425 -0.103345 -0.081264 -0.059184 -0.037101 -0.015013 -0.007257 0.000501
0.008257 0.016011 0.023765 0.031516 0.039266 0.047016 0.054767 0.062518
0.070272 0.078028 0.085786 0.093546 0.101307 0.109070 0.116836 0.124602
0.132367 0.140128 0.151218 0.162304 0.173387 0.184468 0.195549 0.206630
0.217710 0.228790 0.239869 0.250949
0.771439 0.771454 0.771541 0.771727 0.772070 0.772673 0.772976 0.773321
0.773626 0.773905 0.774134 0.774276 0.774329 0.774308 0.774215 0.774049
0.773807 0.773496 0.773137 0.772749 0.772331 0.771877 0.771387 0.770885
0.770396 0.769978 0.769505 0.769148 0.768880 0.768680 0.768534 0.768428
0.768355 0.768307 0.768282 0.768277
0.001249 0.001249 0.001249 0.001249 0.001248 0.001245 0.001243 0.001242
0.001241 0.001239 0.001239 0.001238 0.001237 0.001237 0.001237 0.001237
0.001237 0.001236 0.001236 0.001236 0.001235 0.001233 0.001231 0.001229
0.001227 0.001226 0.001225 0.001224 0.001223 0.001222 0.001222 0.001222
0.001221 0.001221 0.001221 0.001221

```

Figure A2 The streamtube variation data

## APPENDIX B RESULTS USING A 97 X 31 GRID

Results are given for calculations of the flow through Goldman's cascade using a 97 X 31 C-type grid. The effect of including the effects of streamtube contraction on the convergence history is shown in Figure B1, the pressure ratio distribution around the blade is shown in Figure B2, and on the calculated velocity in the blade wake is shown in Figure B3.

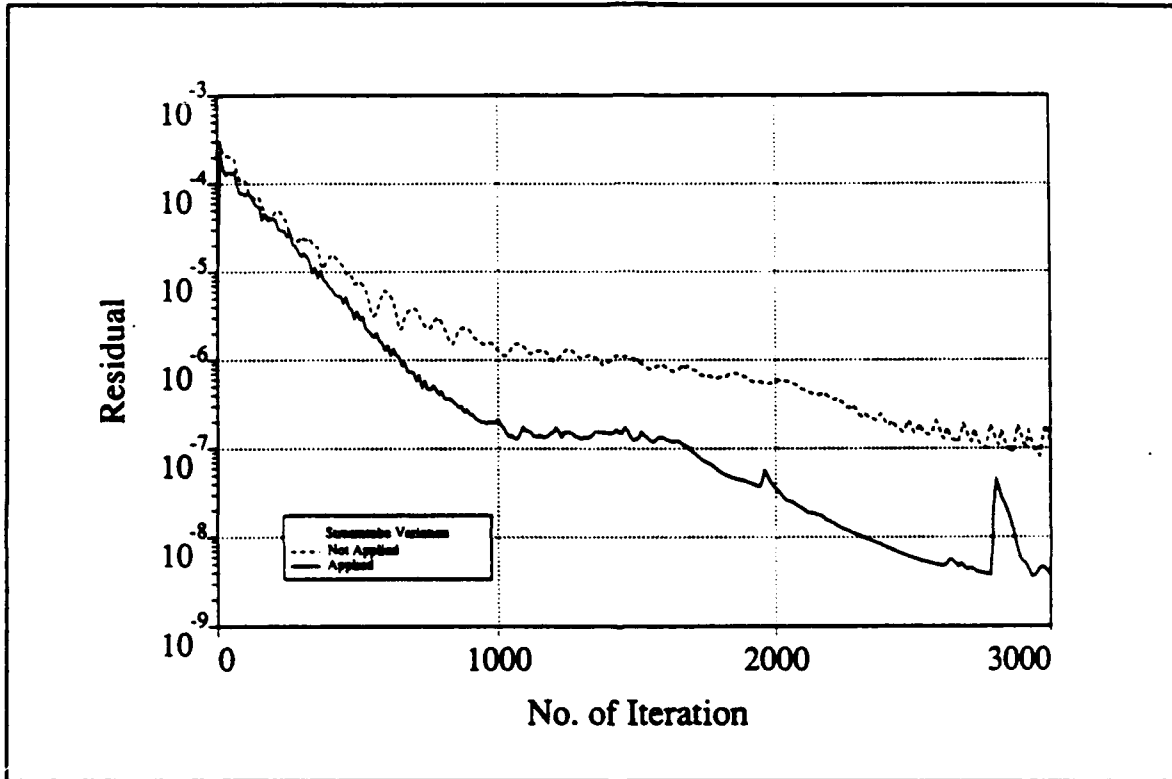


Figure B1 Effect of streamtube variation on convergence history for the 97 X 31 grid

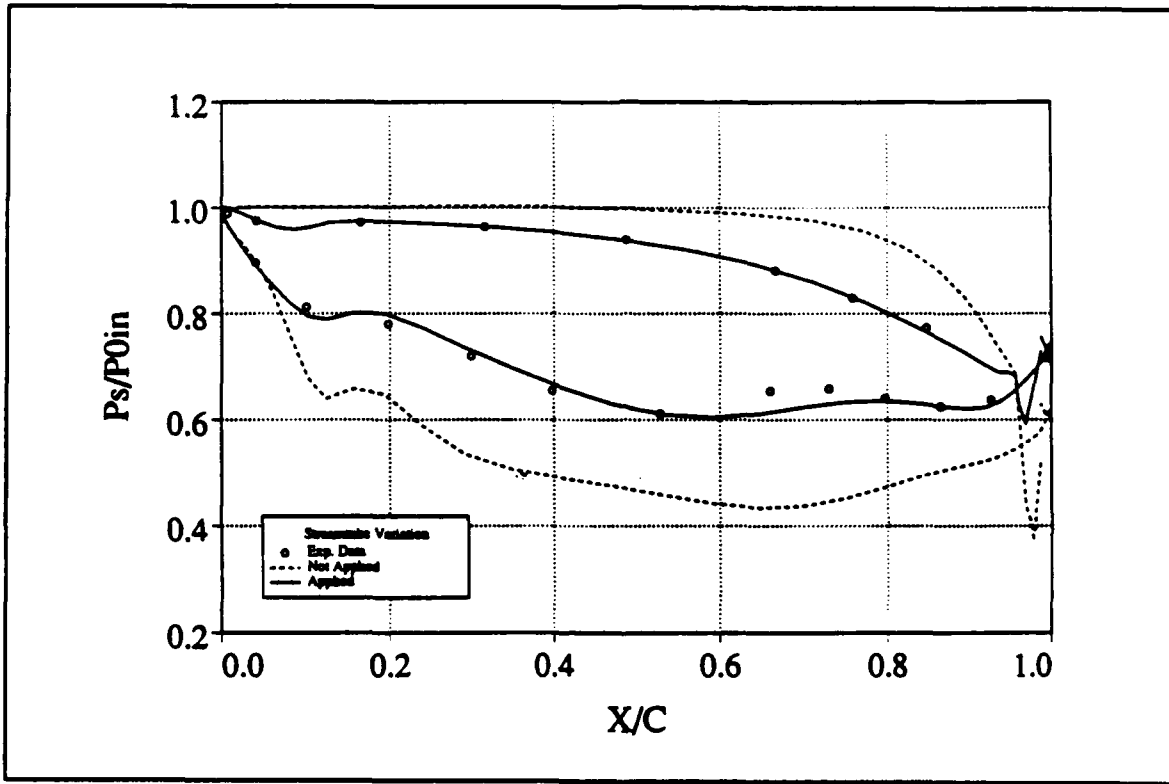


Figure B2 Effect of streamtube variation on static pressure to inlet total pressure ratio

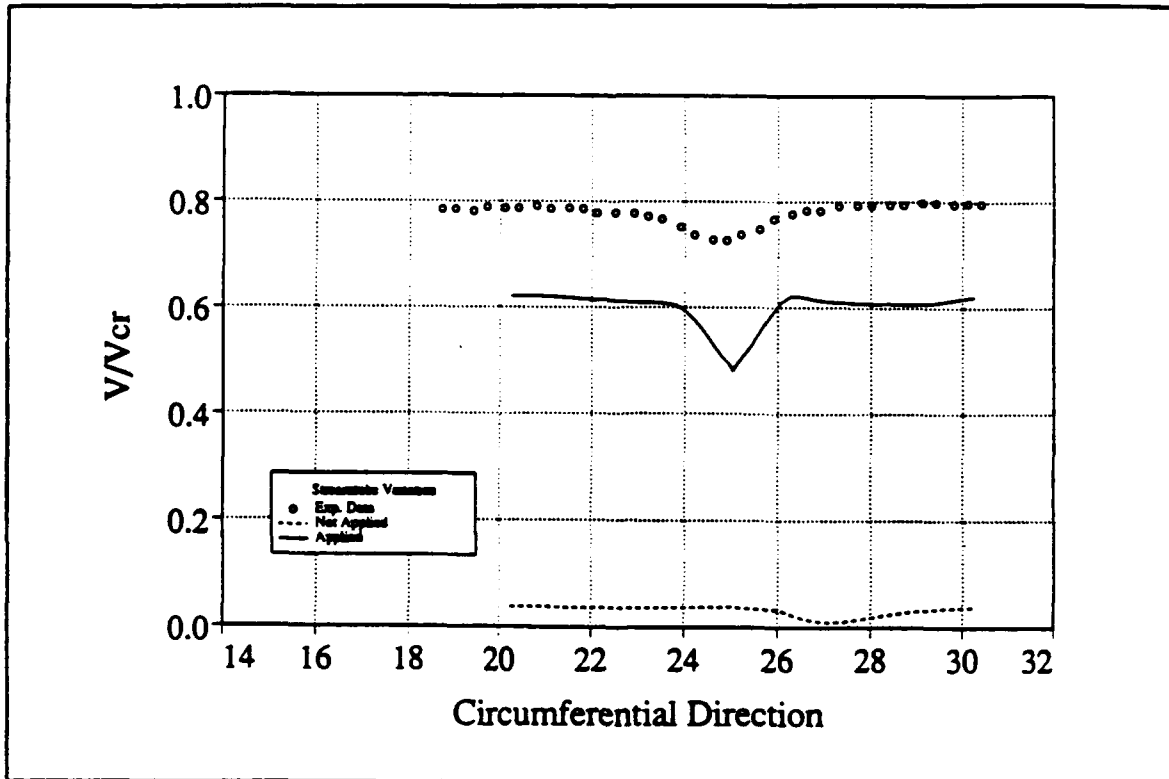


Figure B3 Effect of streamtube variation on wake velocity to critical velocity ratio

## APPENDIX C T106 [Ref. 19] TEST CASE

As another possible test case for the RNG model, a cascade of turbine rotor blades was considered. This section deals with the attempt to establish a baseline solution using the Baldwin-Lomax turbulence model of the extensive experimental data set as presented by Hoheisel [Ref. 19].

The T106 test case is a subsonic turbine cascade which consisted of 7 blades with a chord length of  $c = 100$  mm. The blades had an aspect ratio of 3. A set of experimental data for a Reynolds number of  $5 \times 10^5$  and 0.8 percent inlet turbulence intensity was used in this baseline calculation. The geometry of the turbine blade is shown in Figure C1, with a C-type grid mesh of  $200 \times 30$ .

The RVCQ3D code and an updated version of RVCQ3D, with consistent non-dimensionalization throughout (by Tweedt), were both used to compute the whole flow field. Baldwin-Lomax turbulence modelling was used in each code. The boundary conditions, ambient pressure, total temperature, pressure ratio, the leading edge flow velocity, and the inlet and exit flow angles were provided in the experimental data set. Unfortunately, neither RVCQ3D nor Tweedt's code could satisfy the experimentally measured inlet and exit flow conditions.

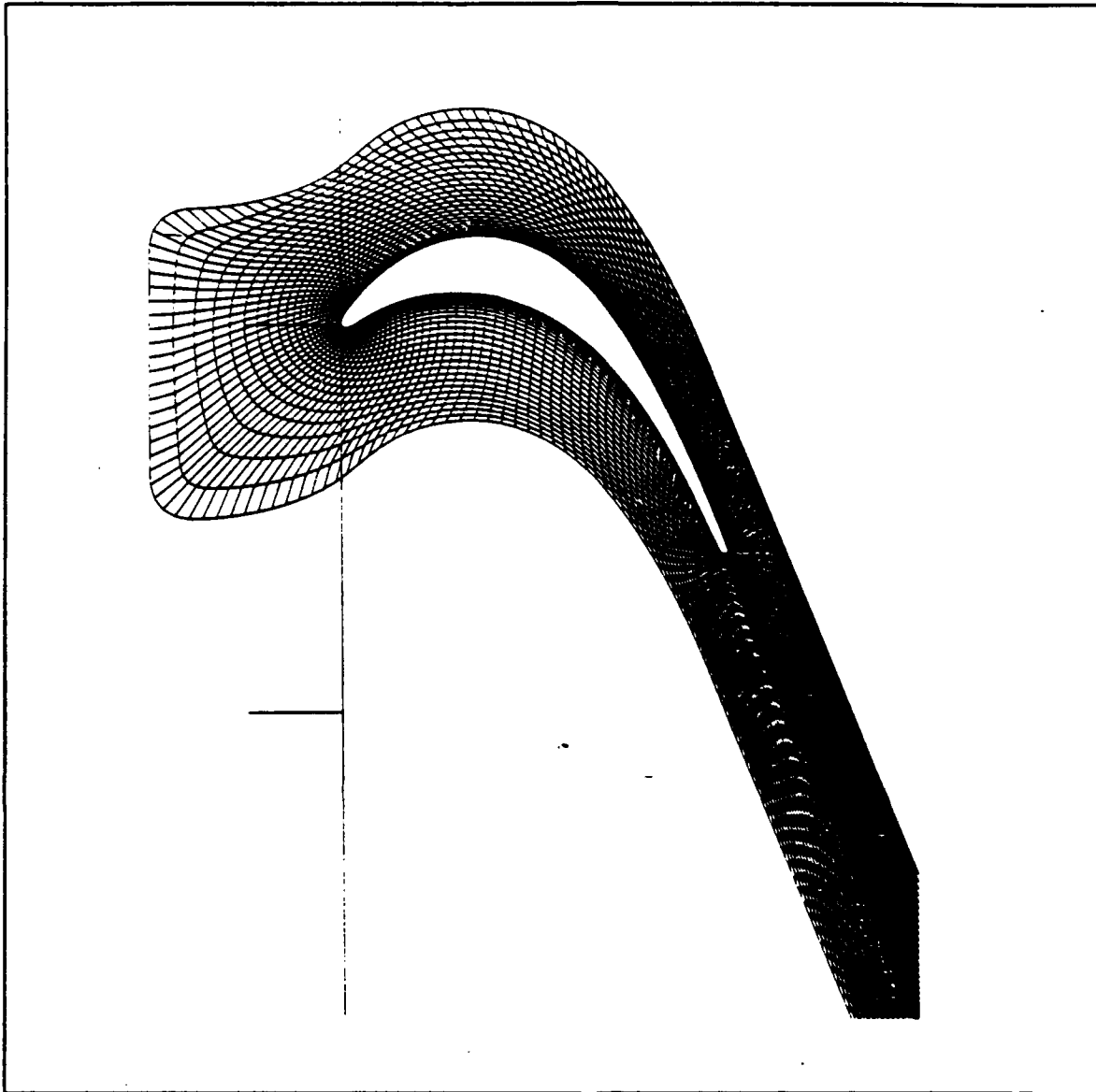


Figure C1 Geometry of the subsonic turbine cascade, T106

The inlet velocity was varied over a wide range of parameters in the experiment. However, the RVCQ3D code could not reproduce complete the isentropic velocity at the inlet boundary.

## 1. Cp COMPARISON

In Figure C2, both codes are seen to generate a better distribution of  $C_p$  on pressure side than on the suction side. Overall, Tweedt's code seems to give better results than the RVCQ3D code.

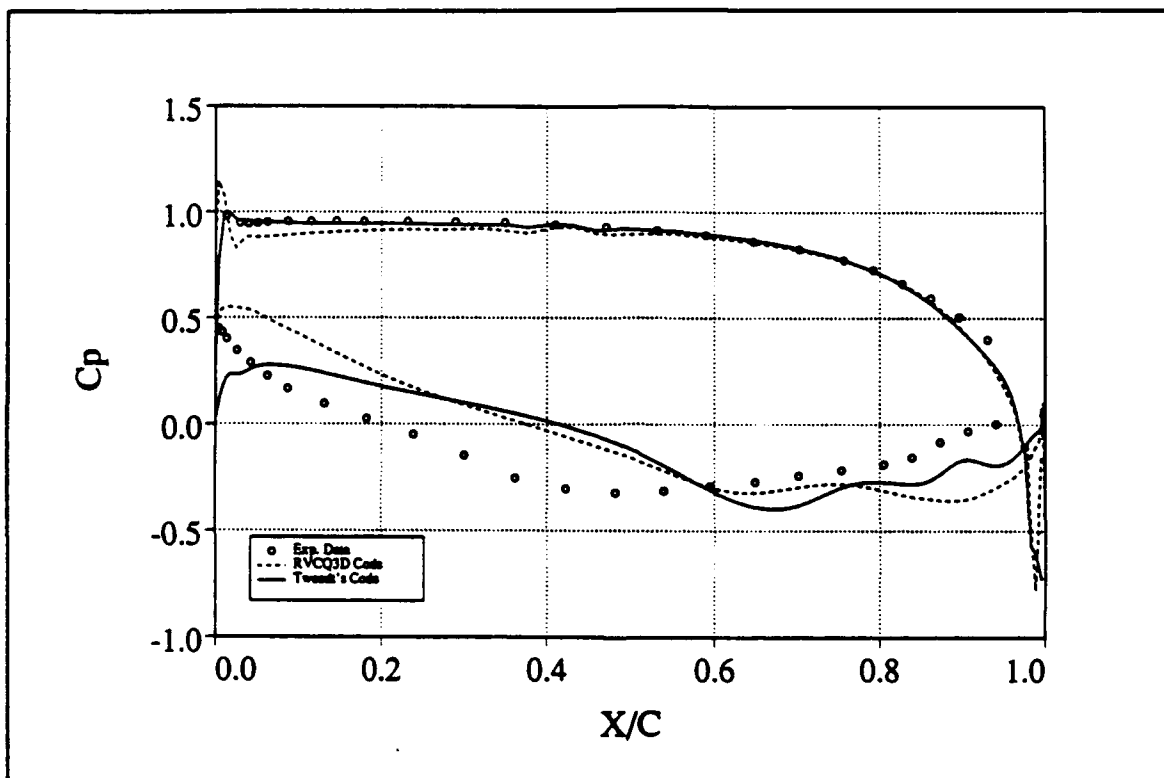


Figure C2 Initial prediction of the blade surface static pressure coefficient distribution around the blade

## 2. SKIN FRICTION COMPARISON

The skin friction coefficient ( $C_f$ ) distribution on the suction side of the blade is shown in Figure C3.  $C_f$  was calculated from the ratio of the shear stress to the local dynamic pressure at the wall. Neither prediction approaches the experimental data.

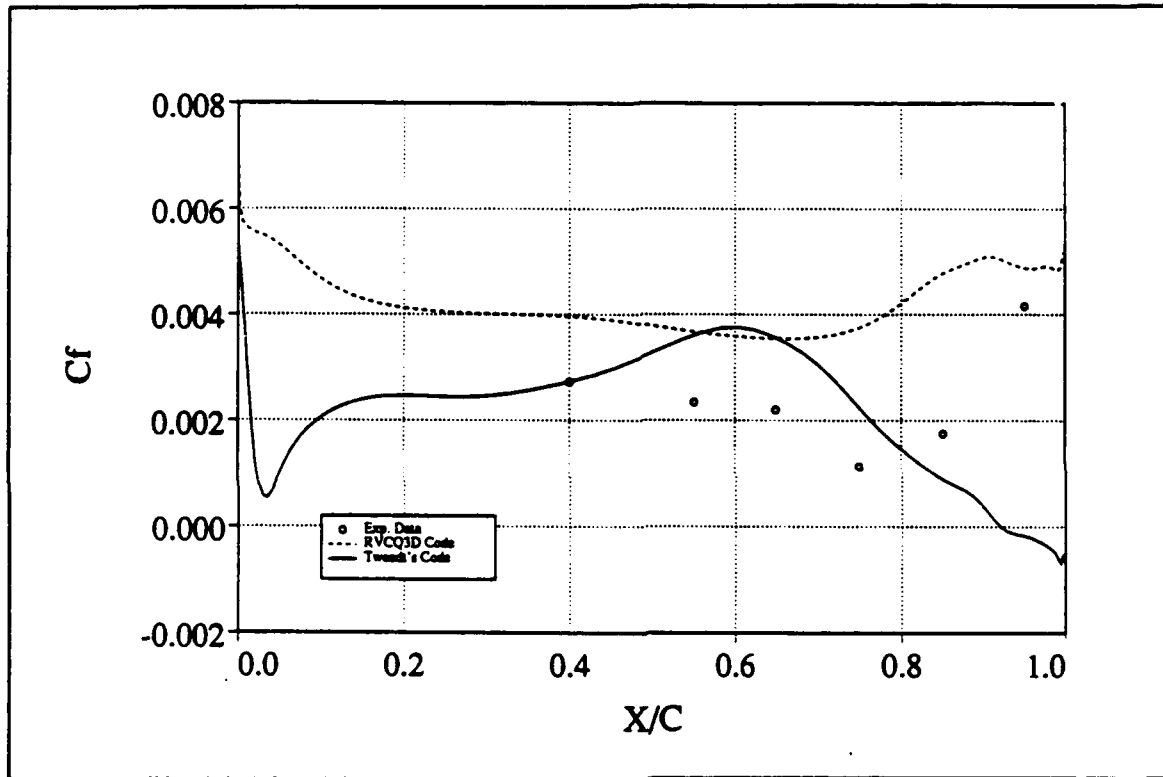


Figure C3 Initial prediction of the skin friction coefficient distribution on the blade surface .

## LIST OF REFERENCES

1. McCOMB, W.D., *The Physics of Fluid Turbulence*, Oxford University Press, New York, 1990.
2. Yakhot, V., and Orszag, S. A., *Renormalization Group Analysis of Turbulence. I. Basic Theory*, Journal of Scientific Computing, Vol.1, No. 1, 1986, pp. 3-51.
3. Lund, T. S., *Application of the Algebraic RNG Model for Transition Simulation*, Purdue University, West Lafayette, Indiana.
4. Kirtley, K. R., *An Algebraic RNG-Based Turbulence Model for Three-Dimension Turbomachinery Flows*, AIAA Paper 91-0172, 1991.
5. Chima, R. V. and Johnson, G. M., *Efficient Solution of Vectorized Multiple-Grid Algorithm*, NASA TM 83376, 1983.
6. Chima, R. V., *Analysis of Inviscid and Viscous Flows in Cascades with an Explicit Multiple-Grid Algorithm*, NASA TM 83636, 1984.
7. Goldman, L. J. and Seasholtz, R. G., *Laser Thermometer Measurements in an Annular Cascade of Core Turbine Vanes and Comparison with Theory*, NASA Technical Paper 2018, June 1982.
8. Hoheisel, H., Klock, R., Lichtfuss, H. J., Fottner, L., *Influence of Free-Stream Turbulence and Blade Pressure Gradient on Boundary Layer and Loss Behavior of Turbine Cascades*, Journal of Turbomachinery, Vol. 109, April, 1987.
9. Liu, J. S., Sockol, P. M., and Prah1, J. M., *Navier-Stocks Cascade Analysis with a Stiff  $k-\epsilon$  Turbulence Solver*, AIAA Paper 88-0594, 1988.
10. Baldwin, B. S. and Lomax, H., *Thin Layer Approximation and Algebraic Model for Separated Turbulent Flows*, AIAA Paper 78-257, 1978.
11. Stock, H. W., and Haase, W., *Determination of Length Scales in Algebraic Turbulence Models for Navier-Stocks Methods*, AIAA Journal, Vol.27, No. 1, Jan., 1989

12. Raj, R. and Lakshminarayana, B., *Characteristics of the Wake Behind a Cascade of Airfoils*, Journal Fluid Mech., Vol.61, Part 4, pp. 707-730, 1973.
13. Sorenson, R. L., *A Computer Program to Generate Two-Dimensional Grids About Airfoils and Other Shapes by the use of Poisson's Equation*, NASA TM-81198, 1980.
14. Chima, R. V., *Revised GRAPE Code Input for Cascades*, NASA Lewis Research Center, June, 1990
15. Chima, R. V., *Explicit Multigrid Algorithm for Quasi-Three-Dimensional Viscous Flows in Turbomachinery*, Journal of Propulsion and Power, Vol. 3, No. 5, Sept.-Oct. 1987, pp.397-405.
16. Chima, R. V., Turkel, E., Schaffer, S., *Comparison of Three Explicit Multigrid Methods for the Euler and Navier-Stokes Equations*, NASA TM-88878, Jan., 1987.
17. Chima, R. V., *RVCQ3D (Rotor Viscous Code Quasi-3-D) Documentation*, NASA Lewis Research Center, August, 1990.
18. Goldman, L. J., *Private Communication*, 1991.
19. Hoheisel, H., *Test Case E/CA-6: Subsonic Turbine Cascade T106*, AGARD-AR-275

### INITIAL DISTRIBUTION LIST

1. Defence Technical Information Center 2  
Cameron Station  
Alexandria, VA 22304-6145
2. Library, Code 52 2  
Naval Postgraduate School  
Monterey, CA 93943-5000
3. Department Chairman, Code AACo 1  
Department of Aeronautics and Astronautics  
Naval Postgraduate School  
Monterey, CA 93943-5000
4. Turbopropulsion Laboratory, Code AAHg 10  
Department of Aeronautics and Astronautics  
Naval Postgraduate School  
Monterey, CA 93943-5000
5. Library 2  
Chung-Cheng Institute of Technology  
Ta-Hsi, Tao-Yuan, 33509  
Taiwan, Republic of China